CHAPTER IV
RESULTS AND DISCUSSIONS

The previous chapter highlighted a step by step experimental procedures followed in preparing the electrodes and electrolytes that were to be used for the supercapacitors fabrication. In this chapter, full discussion about the result obtained will be laid.

4.1 Analysis of the Polymer electrolytes

This section will discuss the results obtained as a result of the experimental procedures of the polymer electrolytes highlighted in chapter III. Specifically the section will discuss the results for the conductivity studies of the sample, its crystal, FESEM and thermal (DSC) analysis.

4.1.1 Conductivity and Chemical Composition Analysis

As mentioned in the methodology chapter, the impedance measurements were carried out using Electrochemical Impedance Spectroscopy (EIS) method using HIOKI 3532-50 LCR Hi-Tester which was connected to a computer. The frequency range of the software was 50 Hz - 1 MHz, and simultaneously calculating both real and imaginary impedance.

Figure 4.1 (a-d) shows impedance plots of a sample of the PSPE containing 0, 20, 40, and 70 wt.% of the H_3PO_4 at room temperatures respectively. At 0 wt.%, of the H_3PO_4, meaning 100 wt.% of PVA, there wasn't any appearance of the semi-circle curve. This can be as a result of absence of the acid in this sample (Fig. 4.1 (a)). The calculated bulk resistance of this sample is very high ($1.15 \times 10^8\ \Omega$) and the conductivity was very low ($2.52 \times 10^{-11}\ Scm^{-1}$) as shown in Table 4.1. However, when the percentage

concentration increases to 20 until 40 wt.%, the bulk resistance decreased gradually thereby resulting in the increase in conductivity of the sample.

The semicircles found on the Fig. 4.1(b) and (c) of the samples containing 20, and 40 wt.% could therefore be connected with the impact of the introduction of the percentage acid and consequently the immobile polymer chain begins to emerge. This also resulted in an increase in their electric conductivities from 8.87×10^{-7} to 1.01×10^{-5} Scm^{-1} and consequent decrease in bulk resistances from 2.10×10^{3} to 1.70×10^{3} Ω in the said samples of 30 and 40 wt.% respectively.

As the acid concentration continues to increase, so the conductivity, thereby making the semicircle disappear, which is an indication that, ions that move around the polymer matrix made resistive component of the polymer electrolytes to exist (Khiar & Arof, 2010; Ulaganathan et al., 2012). Therefore, the bulk resistances obtained for the remaining samples of 50 to 70 wt.% drastically decreases. In fact, at the highest concentration of H_3PO_4, the bulk resistance decreased to 2.58 Ω (as shown in Fig. 4.1(d), while its conductivity increased to 2.56×10^{-3} Scm^{-1}. Details on the results of all the samples are listed in the same table (4.1).

Overall, it can be seen that, there is a strong correlation between the acid concentration (dopants) and the conductivity of the samples of PSPE, in that, the higher the doping the higher the concentration of the PSPE samples. Thus, in terms of conductivity, P0<P10… <P70.

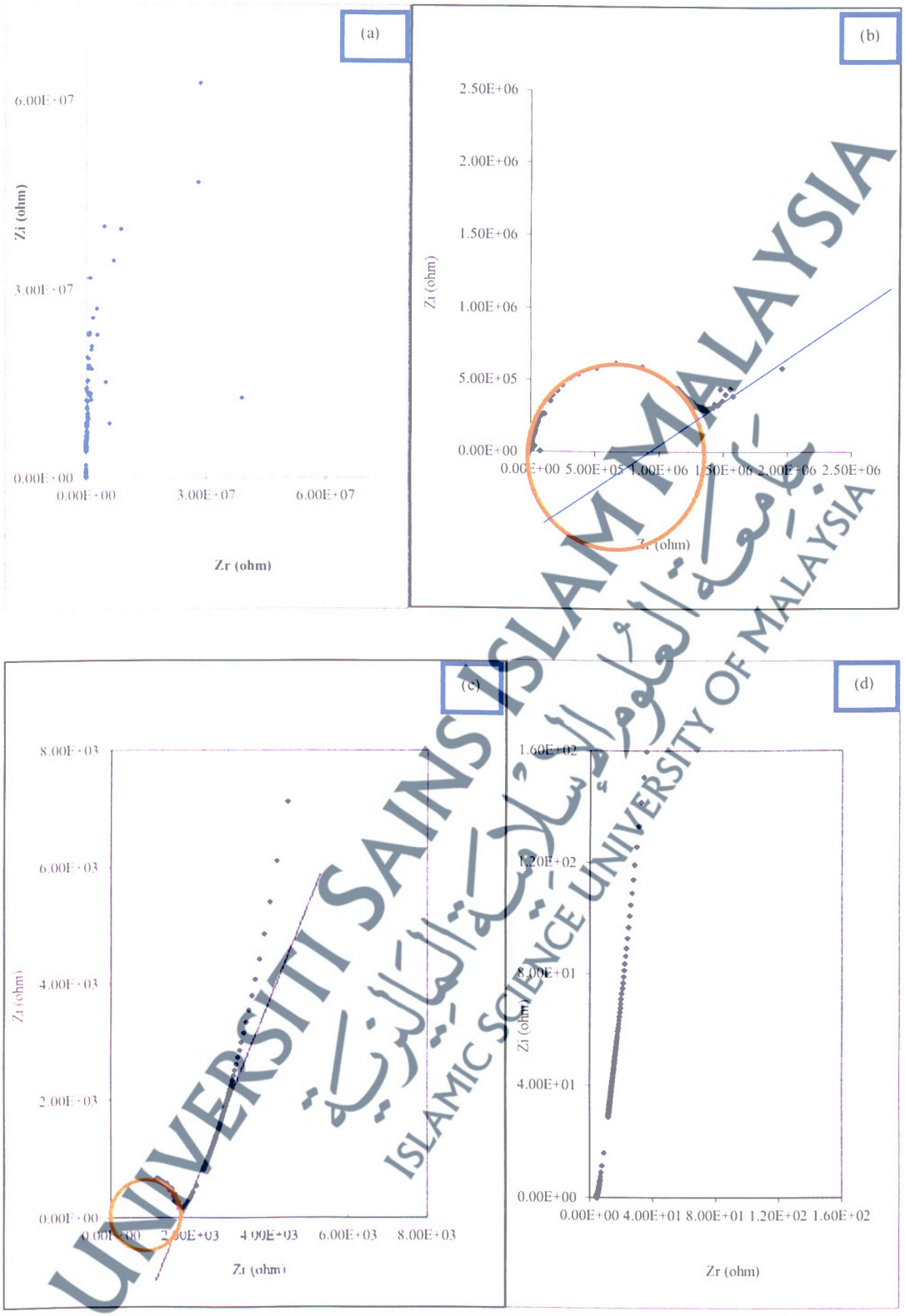

Figure 4.1. Impedance plots of PSPE containing; **(a)** 0 wt.% **(b)** 20 wt.% **(c)** 40 wt.% and **(d)** 70 wt.% of the H_3PO_4 at room temperatures.

Table 4.1 Parameters that Determine the Conductivity in PSPE

Coding	PVA: H_3PO_4	t (mm)(±0.002)	R_b (Ω)	i(Scm^{-1})
P0	100:0	0.009	1.15 x 10^8	2.52 x 10^{-11}
P10	90:10	0.006	1.15 x 10^6	1.74 x 10^{-9}
P20	80:20	0.011	2.40 x 10^4	1.46 x 10^{-7}
P30	70:30	0.005	2.10 x 10^3	8.87 x 10^{-7}
P40	60:40	0.050	1.70 x 10^3	1.01 x 10^{-5}
P50	50:50	0.007	1.93 x 10^1	1.23 x 10^{-4}
P60	40:60	0.026	1.26 x 10^1	6.61 x 10^{-4}
P70	30:70	0.020	2.58 x 10^0	2.56 x 10^{-3}

While Fig. 4.2(a-d) depicts an impedance plots of a samples polymer electrolytes which has cellulose (HSPE) incorporated in it. This figure consist of 0, 10, 50, and 70 wt.% of the H_3PO_4 at room temperatures respectively. Similar to the PSPE, at 0 wt.% (Fig. 4.2 (a)), there affair no any semicircle and the calculated bulk resistance was very high (1.15 x 10^9 Ω), while resulting in a very low electrical conductivity (3.83 x 10^{-12} Scm^{-1}) as summarized in Table 4.2. However, unlike in the case of PSPE samples, when the concentration of the acid of the HSPE was increased to 10 wt.% (Fig. 4.2 (b)), the semicircle started manifesting at the Nyquist plot, which might be as a result of the presence of the immobile polymer chain in the blended solution and porous structure of the cellulose filter paper (Liu et al. 2014). In this case it was observed that, the R_b value for the 10 wt.% decreased to 8.00 x 10^4 Ω. When the substantive amount dopants was added further to the sample in Fig. 4.2 (c) for the sample with 50 wt.%, the semicircle disappeared, given rise to a better conductivity of 8.64 x 10^{-5} Scm^{-1} and very low bulk resistance of 7.37 x 10^1 Ω compared to 20, 30 and 40 wt.%. The sample in Fig. 4.2 (d) (70 wt.%) delivered an outstanding conductivity of 1.67 x 10^{-3} Scm^{-1}, due to optimization of the acid concentrations in this sample. Overall,

as it has been said in the case of PSPE electrolytes, that, there exist a positive correlation between the dopants (H_3PO_4) and the conductivity of the samples of HSPE, because the acid concentration increase with the increase in the conductivity. Thus, in terms of conductivity of HSPE, it can be conveniently writing as H70>H6. ….>H0.

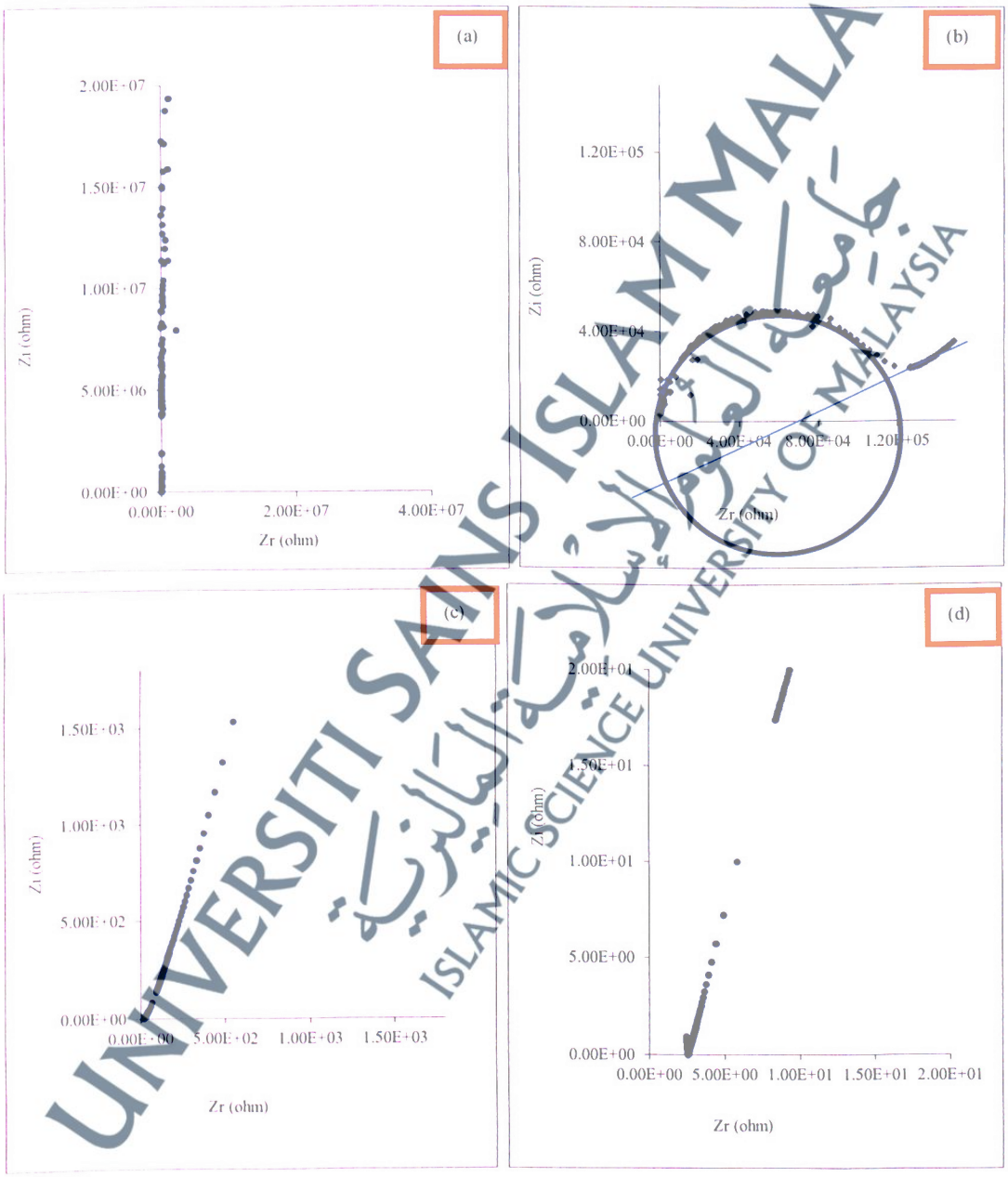

Figure 4.2 Impedance plots of HSPE containing; **(a)** 0 wt.% **(b)** 10 wt.% **(c)** 50 wt.% and **(d)** 70 wt.% of the H_3PO_4 at room temperatures.

Table 4.2 Parameters that Determine the Conductivity in HSPE

Coding	PVA: H_3PO_4	t (mm) (±0.002)	R_b (Ω)	i (Scm^{-1})
H0	100:0	0.013	1.15×10^{9}	3.83×10^{-12}
H10	90:10	0.018	8.00×10^{4}	7.20×10^{-8}
H20	80:20	0.016	1.09×10^{5}	4.73×10^{-8}
H30	70:30	0.017	1.10×10^{3}	5.01×10^{-6}
H40	60:40	0.020	2.10×10^{3}	3.03×10^{-6}
H50	50:50	0.020	7.37×10^{1}	8.64×10^{-5}
H60	40:60	0.019	4.37×10^{1}	1.47×10^{-4}
H70	30:70	0.300	5.73×10^{0}	1.67×10^{-3}

4.1.2 X-Ray Diffraction Analysis

As mentioned earlier, the crystal structure analysis of the solid polymer electrolyte films was examined by a Philip X'Pert X-ray diffractometer (XRD) withCu K_α radiation of wavelength λ=1. 54056 Å for 2θ angles between 10° and 80°.

The XRD analysis was carried out on both the PSPE and HSPE films. After the analysis, the following results were obtained.

The analysis of the structure of the PSPE for 0 wt.% (a); 10 wt.% (b); 20 wt.% (c); 30 wt.% (d); 40 wt.% (e); 50 wt.% (f); 60 wt.% (g); 70 wt.% (h) ratio of the H_3PO_4 was shown in Fig. 4.3.

It can be observed from the semi-crystalline peak of the PVA (2θ=20°) which also affirmed the argument put across by (Hashmi, 2013c) about the semi-crystal behavior of the PVA. The addition of H_3PO_4 causes the decrease in the degree of the crystallinity and consequently the increase in the amorphicity of the material and its conductivity. This result was also in consistence calculated values for the degree of crystallinity of the samples obtained which will be discussed afterward.

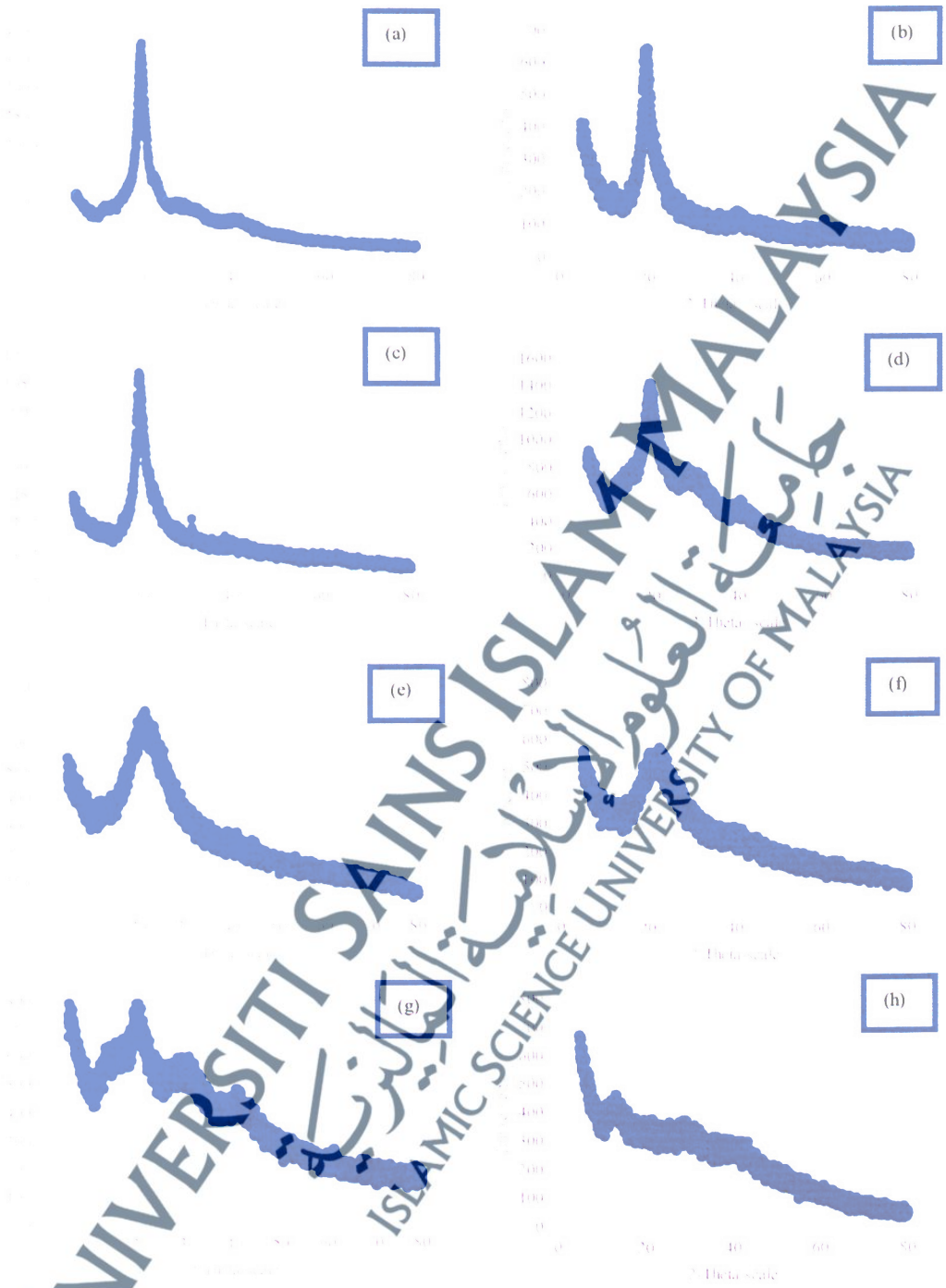

Figure 4.3 XRD Analysis of PSPE containing; **(a)** 0 wt.% **(b)** 10 wt.% **(c)** 20 wt.% **(d)** 30 wt.% **(e)** 40 wt.% **(f)** 50 wt.% **(g)** 60 wt.% and **(h)** 70 wt.% of the H_3PO_4.

Earlier attempts at measuring crystallinity of a samples took place with the work of L. Segal and co-workers 1959 (Marashdeh et al., 2011; Terinte et al., 2011). The so-called peak height method, is an empirical method being the most common and simple method to determine the degree of crystallinity. This method has been widely used for the study of crystallinity of native cellulose.

The crystallinity indices of the PSPE samples were therefore calculated from the the equation stated earlier in methodology (equation 3.3) and the resulting percentage of degree of crystallinity is shown in Table 4.3. It can be seen from the table that, sample P0 has the highest degree of crystallinity of 42.6 %, which is almost of in agreement with what was obtained by Guirguis & Moselhy (2012) for a 100 % PVA. However, as the concentration of the acid increases the percentage crystallinity of the sample increase. Hence, this result compliment that of conductivity result for a conductivity of the sample that was summarized in the earlier Table 4.1. The lower the degree of crystallinity, the higher the conductivity. The result was also in consistent with XRD pattern of the samples, as the XRD peaks decrease so the percentage crystallinity.

Table 4.3 Degree of Crystallinity of PSPE

Sample	PO	P10	P20	P30	P40	P50	P60	P70
Crystallinity (%)	42.6	40.2	38.2	34.0	31.1	28.0	26.2	23.1

Furthermore, the analysis of the structure of the HSPE which are all cellulose incorporated based samples for 0 wt.% (a); 10 wt.% (b); 20 wt.% (c); 30 wt.% (d); 40 wt.% (e); 50 wt.% (f); 60 wt.% (g); 70 wt.% (h) ratio of the H_3PO_4 is shown in Fig. 4.4 (a-i). It can be observed from the semi-crystalline peak of the PVA at 2θ approximately equal to 22° decreases with the decrease in the crystallinity percentage and increase in the acid concentration. The behavior of the peaks also is in consistence

with the earlier argument put across by (Hashmi, 2013c) regarding the semi-crystal behavior of the PVA. The border humps at the left and right hand sides at 2θ= 14.8, 16.2 and 33.8 (approx.) across all the sample are of the cellulose crystalline form and are consistent with the previous report by Qiu et al. (2014).

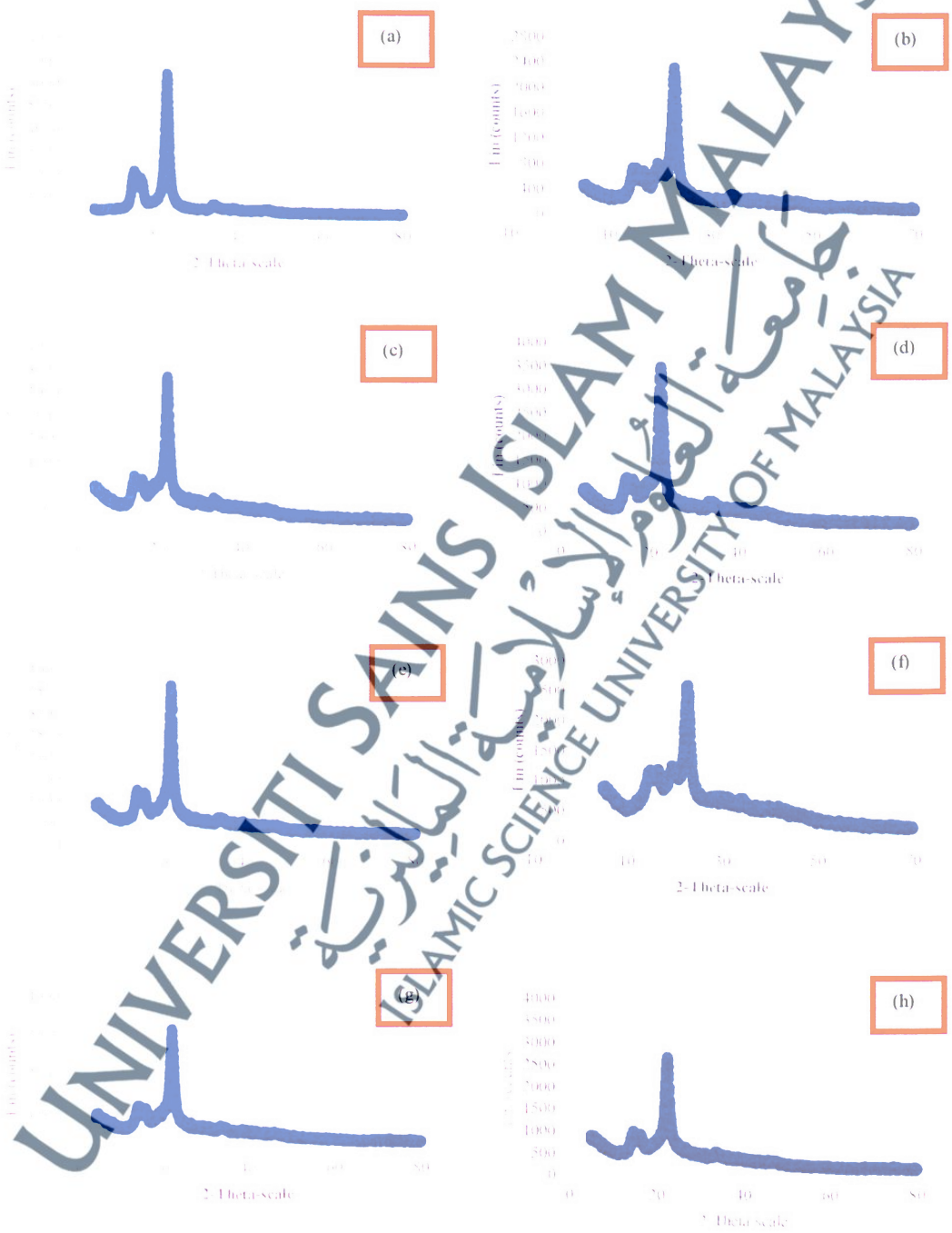

Figure 4.4 XRD Analysis of HSPE containing; **(a)** 0 wt.% **(b)** 10 wt.% **(c)** 20 wt.% **(d)** 30 wt.% **(e)** 40 wt.% **(f)** 50 wt.% **(g)** 60 wt.% and **(h)** 70 wt.% of the H_3PO_4.

Furthermore, the crystallinity indices of the HSPE samples were also calculated from the earlier equation and the resulting percentage of degree of crystallinity is shown in Table 4.4. From the table, it can be seen that, overall, the results of the degree of crystallinity are less than that of PSPE. This is due to the presence of the cellulose in the sample. The decrease in the CI_n values from sample H0 to H70 were associated with the continuous doping of the H_3PO_4 into the sample. Thus, while H0<H10… <H70, for the conductivity, conversely, H0>H10… >H70 in the case of degree of the crystallinity.

Table 4.4 Degree of Crystallinity of HSPE

Sample	HO	H10	H20	H30	H40	H50	H60	H70
Crystallinity (%)	24.3	21.0	20.0	19.1	17.2	16.3	14.7	11.9

4.1.3 Field Emission Scanning Electron Microscope (FESEM) Analysis

Both PSPE and HSPE films have been examined using different magnifications. The resulting images are shown in Fig. 4.5 and 4.6.

Figure 4.5 is the FESEM of the selected images of PSPE containing 0 and 40 wt.% at a magnification of x30 (1.00 mm) are shown in Fig. 4.5 (a). It can be observed that, there is no any obvious particles or patterns that is sited in these images, this is because they are all blended colorless reagents that were allowed to dry so nothing can be sited. These micrographs remained the same for the whole samples of PSPE. The idea behind their inclusion in this work is being able to observe the differences between them and those of cellulose incorporated sample and to be able to ascertain whether or not there is any correlation between the FESEM of the samples and their electrical conductivity. However, while the micrographs clearly shows that the two different types of the sample (PSPE and HSPE) differ in the appearances, there is

no clear evidence that shows the FESEM of the whole PSPE samples has any correlation with conductivity studied so far.

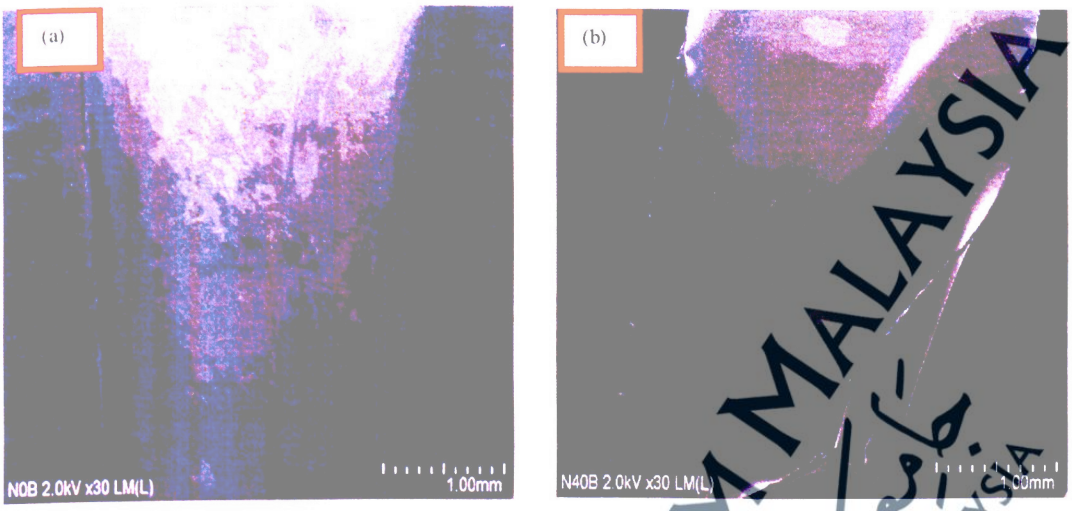

Figure 4.5 FESEM images of PSPE containing **(a)** 0 wt.% and **(b)** 40 wt.% at a magnification of x30 k (1.00 mm).

In Figure 4.6 the FESEM images of HSPE containing 20,50 and 70 wt.% of the H_3PO_4 was displayed at magnifications of 3.5 mm x 300 k. Cellulose filter paper is comprised of wood–cellulose fibers which have a high aspect ratio and porous structure capable of allowing the ionic movements across the polymer electrolyte.

The micrograph of samples with 20 and 70 wt. % shows an entangling mat nature, indicating the presence of cellulose filter paper in those compositions. The images show an even distribution of the blended PVA/H_3PO_4. These images look fairer suggesting that the cellulose filter paper soaked in the prepared compositions of the PVA/H_3PO_4 liquid electrolyte was not "well-soaked" as such, some little holes are sited in the images. However, unlike images in Fig. 4.6 (a) and (c), the image of sample in the Fig. 4.6 (b) looks darker indicating that the cellulose is well-soaked in the homogenous solution of liquid electrolyte before drying. Normally, after soaking, cellulose fibers become coated with polymer, as a result the fibers become thicker and

also the fibers in the inner layers become less visible as shown in Fig. 4.6 (b). Overall, although, some diffused features are visible in the uncoated cellulose membranes due to the presence of some open fibrils, but the fibers are apparently smoothened due to the coatingng of the open fibrils with PVA/H_3PO_4 blends.

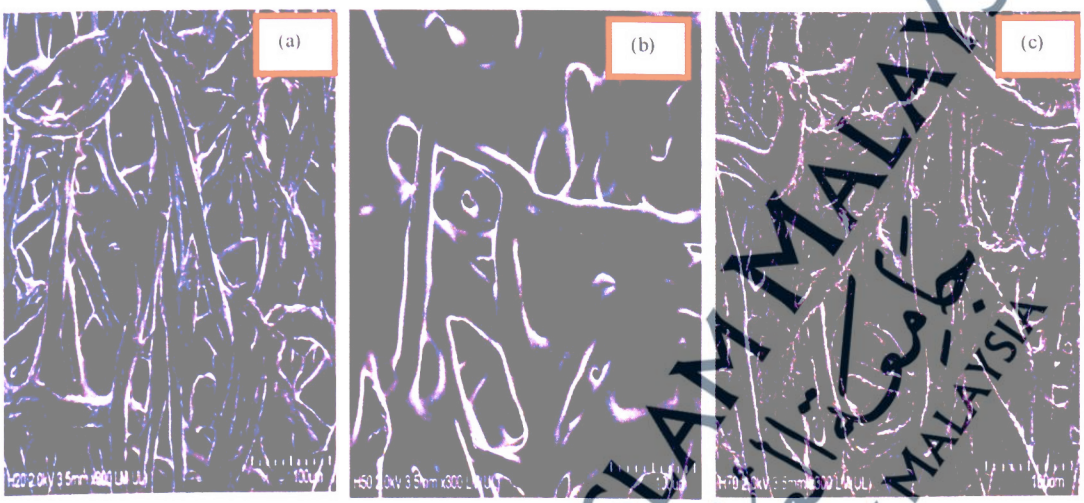

Figure 4.6 FESEM Images of HSPE containing **(a)** 20 wt.% **(b)** 50 wt.% and **(c)** 70 wt.% **(c)** at the magnification of 3.5 mm x 300 k.

4.1.4 Differential Scanning Calorimetry Analysis

DSC is a technique that provides information such as glass transition *(T_g)*, melting *(T_m)* and crystallization *(T_c)* temperatures, in addition to the associated enthalpy for each process of a particular sample.

As earlier stated in the methodology, that, the samples for DSC measurements were prepared from several tiny rectangular pieces cut from the polymer film to a mass ranging from 1.98 -24.24 mg (±0.02) for PSPE and 7.08 – 19.82 mg (±0.02) for HSPE. The temperature range studied was 40 to 300 °C. The heating/cooling rate was 10 °C/min. The aforementioned temperature was selected due to the fact that, the majority of the DCS analysis of PVA is set to a maximum temperature of 300 °C since

even the highest transition temperature of PVA will hardly exceed 250 °C, noting the theoretical value of its thermal transition is 230 °C (Othman et al., 2011).

The DSC technique has been performed to observe the change in transition temperature that is caused by the doping. Starting with PSPE as summarized in Table 4.5, for the sample that is 100 % PVA (P0), the value of T_g was 89 °C, which is nearly in agreement with that reported previously in the literatures (Guirguis & Moselhey, 2012). However, the value obtained for the T_m (223.5 °C) is close to the theoretical value of pure PVA. Furthermore, it can be seen that, the next two samples show a very good thermal transition, (T_m) with an endothermic peak of slightly above 200 ^{0}C (i.e. 221 and 207 for P10 and P20 respectively) which indicates the huge percentage weight of PVA is present. Noting the theoretical value of the thermal transition of the pure PVA as 230 ^{0}C, this result is closely related to that, and was in agreement with that of (Agrawal, 2004; Jelinska et al., 2010; Othman et al., 2011). However, probably due to the presence of chemical content, or intermolecular interaction (Mudigoudra et al., 2012) form among PVA and H_3PO_4, the thermal transition starts to decrease with the increase in temperature.

It is interesting to show how the thermal transition of PVA varies after doping the different concentrations of H_3P0_4. One key aspect is the determination of whether the resulting blend samples result miscible or not (Guirguis & Moselhey, 2012). The higher the melting point temperature the more the stability of the molecules therein, thus, pure PVA has more stable molecules than PVA/H_3PO_4 composite. So, it can be seen that the T_m and T_c decreases (or even diminishes) as the concentration of the acid increase. This is a known fact that in homogenized blends, the melting shifts to the lower level (Othman et al., 2011; Guirguis & Moselhey, 2012). Also the theoretical

glass transition of the PVA alone is about 85 °C while the composite shows down and upwards shifts of this temperature. This could not be unconnected with the gradual increment in the concentration of the acid and instability of molecules of PVA/H_3PO_4.

Table 4.5 Parameters for the Thermometric Analysis in PSPE

Coding	PVA: H_3PO_4	Mass (mg) (±0.02)	Temperature (^{0}C)		
			T_g	T_m	T_c
P0	100:0	1.98	89	223	152
P10	90:10	4.48	81	221	166
P20	80:20	7.41	127	207	186
P30	70:30	8.27	117	156	-
P40	60:40	15.12	116	155	-
P50	50:50	13.53	101	164	160
P60	40:60	19.48	63	160	150
P70	30:70	24.40	79	129	79

Table 4.6 summarizes the DSC analysis result for the HSPE containing 0 to 70 wt.% ratio of the H_3PO_4 in a PVA/H_3PO_4 blend. From the Table it can be seen that, unlike P0 which completely PVA, the effect of cellulose filter paper in H0 has made its T_g value to be enhanced to 98 °C, although this result also coincides with the T_g value of 100 % percent of PVA. However, the value obtained for the T_m (218 °C) – which is also less than that of P0- is close to the theoretical value of pure PVA. Differences in the area of the melting endotherm are also noticed. The melting point is a physical parameter used to identify the nature of the substance and its degree of purity. The data in Table indicate that the melting point *(T_m)* for the blend samples are closing showing the presence of PVA in the blend. The crystallization (T_c) for the samples H20 to H70, perhaps due to the increment of the concentration in the sample.

Table 4.6 Parameters for the Thermometric Analysis in HSPE

Coding	PVA: H_3PO_4	Mass (mg) (±0.02)	Temperature (^{0}C)		
			T_g	T_m	T_c
H0	100:0	7.08	98	215	165
H10	90:10	8.58	81	172	95
H20	80:20	14.63	127	165	-
H30	70:30	12.08	118	168	-
H40	60:40	12.08	116	159	-
H50	50:50	8.65	101	117	-
H60	40:60	19.82	96	150	-
H70	30:70	8.80	84	111	-

The importance of polymer electrolytes in nowadays technology cannot be over emphasized. From the foregoing discussion the noble performances of PSPE and HSPE were highlighted. Their measurements which were carried out at room temperature and for used as an electrolyte were prepared from the composition of PVA and H_3PO_4, with, the PVA samples kept constant while varying the H_3PO_4 at 0, 10, 20, 30, 40, 50, 60, and 70 wt.% (for PSPE) and immerse in a cellulose filter paper (for HSPE). Both PSPE and HSPE showed an excellent result of 2.56 x 10^{-3} Scm^{-1} and 1.67 x $10^{-3.}$ Scm^{-1} respectively at the optimum concentration of H_3PO_4 (70 wt.%) in each blend. Furthermore, from the overall results of the XRD analysis carried out on both categories of the samples revealed a semi-crystalline peak of the PVA decreases as the acid concentration increases. Which in turns indicated that, there is an enhancement in the amorphicity of the samples responsible for the process of ion transport. Furthermore, the degree of crystallinity calculated from the XRD peaks revealed that, the lower the degree of crystallinity, the higher the conductivity. Hence, the result was in consistent with XRD pattern of the samples, as the XRD peaks decrease so the percentage crystallinity. This characteristic behavior was confirmed from the analysis of the

differential scanning calorimetry results. FESEM result pictured the entangling nature of the combined samples as a result of the presence of the cellulose filter paper in HSPE while a clear (no particles sited) in PSPE.

In the next section, the fabrication and characterization of CPCMWCNTs with and hybrid polymer electrolytes as separators will be discussed. It could be recalled in chapter III, which discussed the experimental procedures taken to ensure an outstanding results, it was further explained that, of the three commercial CNTs (i.e. Carboxyl, Hydroxyl and Normal CNTs), nine different supercapacitor cells were prepared (three cells from each powdered CNTs). This section will provide detailed discussions of each of the cells fabricated from each of the electrodes. This entails mainly the characterization and measurements of all the fabricated cells.

4.2 Fabrication and Characterizations of Supercapacitor Based on the Commercially Prepared Carboxyl Multiwalled Carbon Nanotubes (CPCMWCNTs) and Hybrid Solid Polymer Electrolytes (HSPE)

4.2.1 Microstructure Characterizations

As it was disclosed earlier, XRD spectra were obtained with an XRD (Philip X'Pert XRD with Cu K_α radiation of wavelength λ=1. 54056 Å for 2θ angles between 10° and 80°) that used Cu Kα radiation (λ = 1.5406 Å) operating at 40 kV and 30 mA.

The XRD analysis of the C90PVdF-HFP10 electrode as depicted in Fig. 4.7 show all the diffraction peaks clearly. The XRD peaks that appear in $2\theta = 26^0$ and $2\theta = 43^0$ (red vertical lines) might be as a result of the hexagonal structure of (002) and (101) respectively, which indicates that the Carboxyl MWCNT have high conductivity (Dong et al., 2007). In addition, there appeared a wider diffraction at 2θ=20. 1^0 (blue vertical line) correspond to crystalline peaks of PVDF (Stolarska et al., 2007). These results, also proved well by the same result of the XRD obtained by many researchers such as (Stolarska et al., 2007; Li et al., 2010).

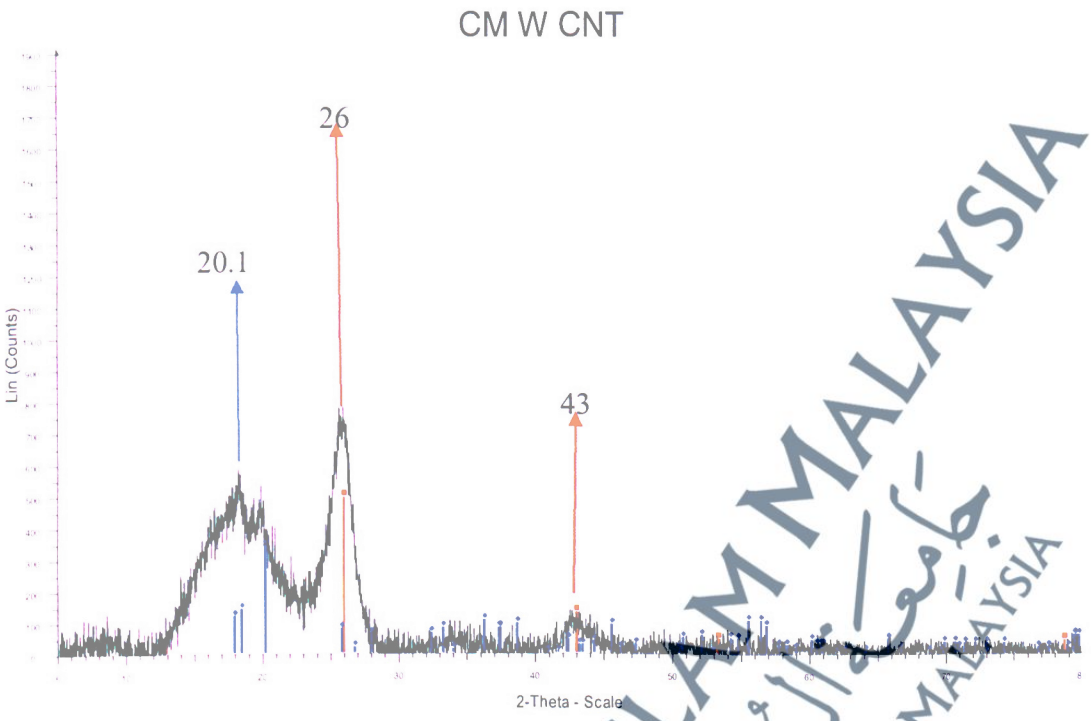

Figure 4.7 XRD plot of C90PVdF-HFP10 electrode with red and blue vertical lines. The red vertical lines indicate the presence of CNT while blue indicating the presence of crystalline PVdF.

Furthermore, the surface morphology of the sample which was investigated using FESEM for images in Fig. 4.8 (a) and (b), of CPCMWCNTs of pure (free) CPCMWCNTs and sample electrode with 90 wt.% of CPCMWCNTs (C90PVdF-HFP10) are shown. Pure CPCMWCNTs exhibits regular, entangled and smooth surface morphology with the outer diameter of ~30 nm and length of several micrometers. The few larger tubes that were cited in the FESEM structure indicate that the original MWCNTs has been oxidized thereby resulting in the enlargements of the tubes. However, the FESEM image in Fig. 4.8 (b), although was clearer, but it is not as the case of Fig. 4.8 (a), which is as a result of the addition of 10 wt.% binder into the composition of the electrode.

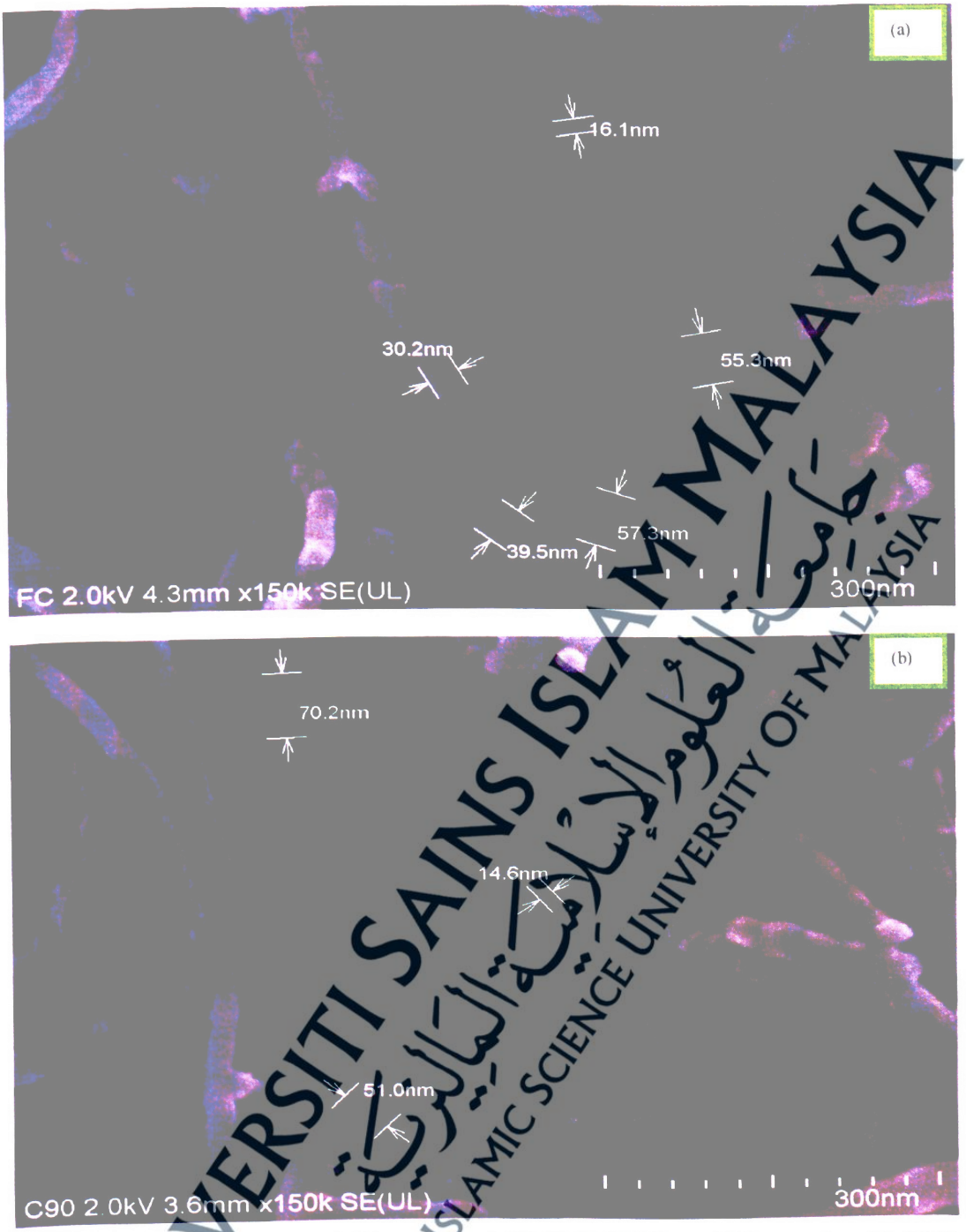

Figure 4.8 FESEM images of **(a)** pure (free) CPCMWCNTs and **(b)** sample with 90 % CPCMWNTs showing an average outer diameter of the tubes. The magnifications of the two samples were 4.3 mm x 150 k and 3.6 mm x 150 k respectively.

Lastly, Fig. 4.9 depicts the FESEM images of C90PVdF-HFP10 electrode overlapped on HSPE containing 60 wt.% of H_3PO_4 (i.e. H60) at the magnifications of 2 kV x 45 k (1.00 μm). The image was taken at an angle of 30^0 in order to see the

boarder where the electrode and electrolyte interface. Here it can be deduced that, the thinner the electrode the better, so, thicker electrodes will not only leads to bulky construction of the cell, but also result in higher internal resistance as ions would not be able to diffuse thoroughly from one barrier of the electrode to the other. It was stated in the literature review how different researchers emphasized and recommended that for a high capacitance to be realized, especially in a flexible-type cell, a thinner-liked electrode should be constructed.

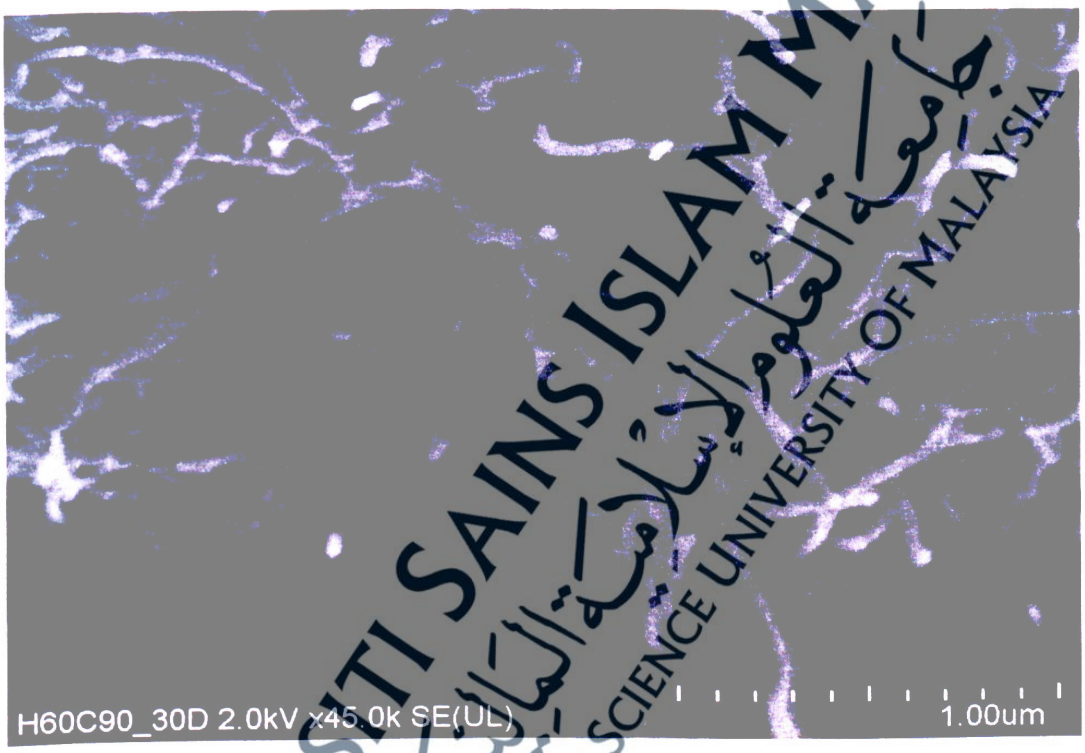

Figure 4.9 FESEM images of C90PVdF-HFP10 electrode overlapped on HSPE containing 60 wt.% of H_3PO_4, 90 wt.% of CPCMWCNTs at the magnifications of 2.0 kV x 45.0 k (1.00 µm) and an angle of 30^0.

4.2.2 Thermogravimetric Analysis (TGA)

The thermogravimetric analysis (TGA) was carried out in the scale-range of 50 ^{0}C to 1000 ^{0}C under nitrogen gas (N_2) flow at a heating rate of 10 ^{0}C min^{-1} on a METTLER, STAR^e SW 10.00 thermal analyzer in line with our previous work (Hashim et al., 2014). The thermal stability of the samples was discerned in Fig. 4.10. These figures include

(a) 0 % sample (Background) (b) pure CPCMWCNT and (c) C90PVdF-HFP10 – Double scale.

Before beginning the experiment a background heating was done in order to clear any ruminant residue and for re-calibration (Fig. 4.10 (a)). Trace in Fig.4.10 (b) shows the pure CPCMWCNT with major loss of just 11.1 % occurring at 611.8 ^{0}C leaving a residue of 87.9 %. This result shows that the pure MWCNTs have very good thermal stability and consequently, good in application of electrochemical devices. While in Fig. 4.9 (c), it can be noticed that, when the active materials were all incorporated in a single electrode, three losses were recorded. The initial loss of 2.5 % of the total samples occurs at 307.2 ^{0}C, then the second loss of 5.9 % happened at 449.5 ^{0}C and the highest loss of 11.6 % was noticed at 708.8 ^{0}C. This shows that the overall active material will work well in supercapacitor fabrication.

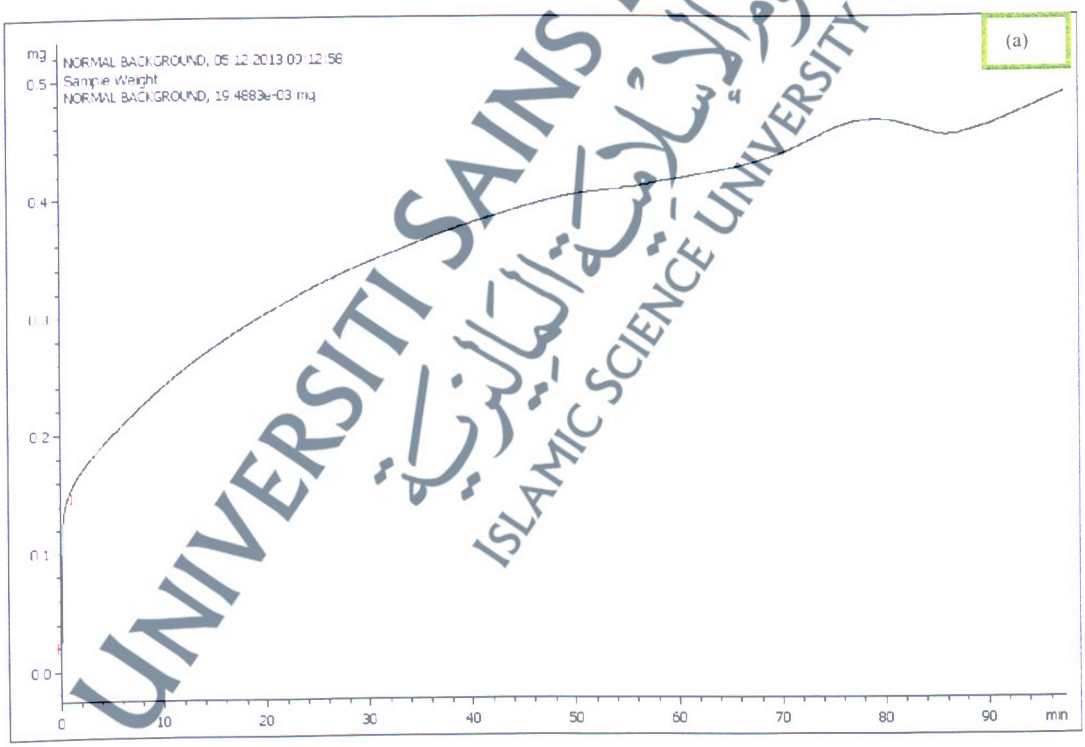

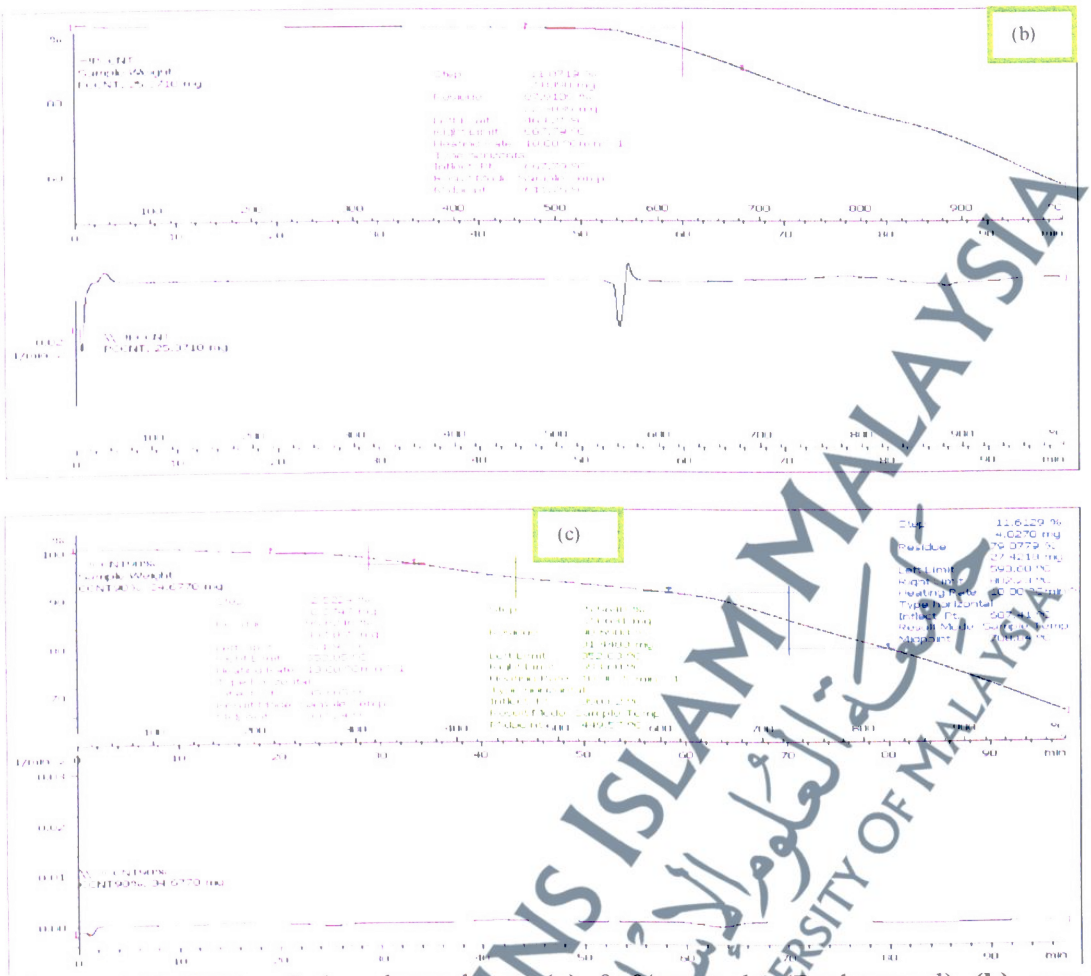

Figure 4.10 TGA of the electrode at **(a)** 0 % sample (Background) **(b)** pure CPCMWCNT **(c)** C90PVdF-HFP10 – Double scale.

4.2.3 Electrochemical Behavior

It can be recalled during the conductivity studies of the polymer electrolytes, it was mentioned that, three most effective samples in terms of conductivity among the cellulose incorporated electrolytes (HSPE) were selected for the fabrication of the supercapacitor cell. They are the samples with 50, 60 and 70 wt.% of the orthophosphoric acid, which also coded as H50, H60 and H70 respectively. The electrochemical behaviors of cells constructed by sandwiching the electrode and electrolyte using two-electrode system is therefore investigated by CV and CD measurements.

Figure 4.11 shows CV of Cell –A (C90PVdF-HFP10 |H50| C90PVdF-HFP10) at the scan rates of10, 50 and 100 mV, within a voltage window of 0.0 – 1.0 V. It can be discerned that the resulting CV curves of the cell displayed a leaf-like and mirror symmetric indicating though, a modest supercapacitive behavior for CPCMWCNTs that uses an aqueous electrolyte of 50 wt.% of H_3PO_4 in homogenous solution of PVA/H_3PO_4.

From the calculation (using the equation 3.4 stated earlier), it could be obtained that the specific capacitance is 8, 11 and 19 Fg^{-1} for a scan rate of 100, 50 and 10 mV, respectively as shown in Table 4.7. From these results it can be deduced that, there is a relationship between the capacitance and scan rate. The specific capacitance decreases from 19 Fg^{-1} to 8 Fg^{-1} which could be attributed to the slow transfer of ions on the electrode electrolyte interface (Shu et al., 2013). It is also important to note that, the lower conductivity of the electrolyte film can lead to lower capacitance. The film H50, which was used as a separator has the conductivity of 8.64×10^{-5} Scm^{-1}, this is another evidence for the resulted low capacitance of the cell.

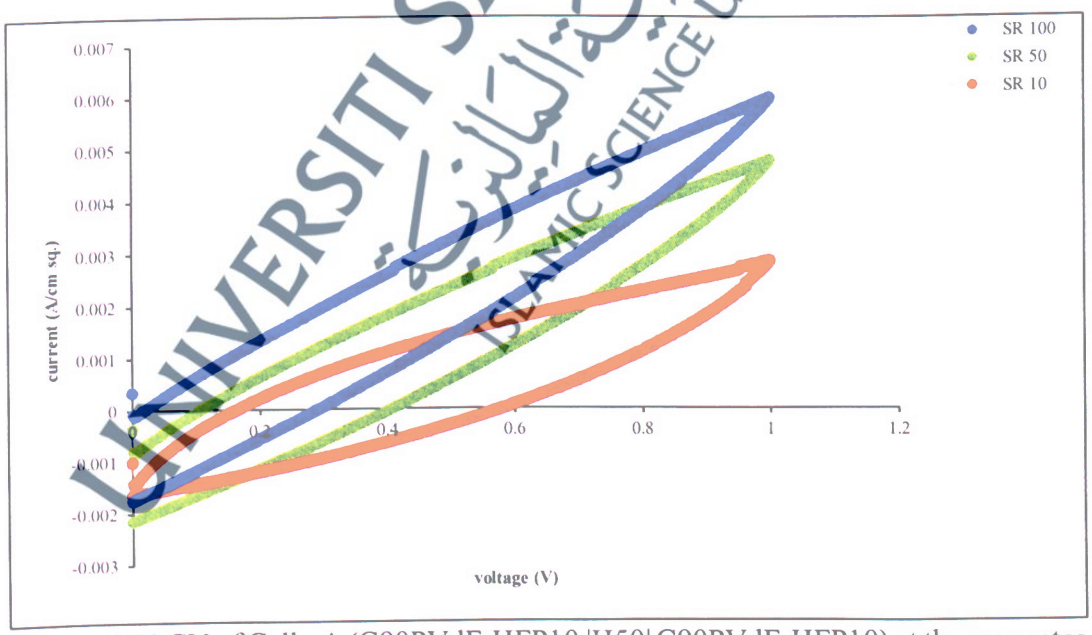

Figure 4.11 CV of Cell –A (C90PVdF-HFP10 |H50| C90PVdF-HFP10) at the scan rates of 10, 50 and 100 mV.

Table 4.7 CV Performances of cell-A (C90PVdF-HFP10 |H50| C90PVdF-HFP10)

Cell	Working voltage (V)	Capacitance value of different scan rates (Fg^{-1})		
		100 mV	50 mV	10 mV
A-C90H50	1	8	11	19

Furthermore, Fig. 4.12 also shows CV of Cell–B (C90PVdF-HFP10 |H60| C90PVdF-HFP10) at the scan rates of10, 50 and 100 mV for a voltage window of 0.0 – 1.0 V. Noting from this cell, the electrolyte used in this cell (H60), its specific capacitances improved remarkably to 16, 19 and 23 Fg^{-1} for scan rates of 100, 50 and 10 mV respectively (see Table 4.8). These results almost double that of cell-A, which might be attributed to the increase in ionic conductivity in the polymer electrolyte of the HSPE. Unlike the curves of cell A, the resulting CV curves of this cell displayed a better leaf-like and mirror symmetric indicating an ideal supercapacitive behavior for a CPCMWCNTs that uses an aqueous electrolyte of 60 wt.% of H_3PO_4 in homogenous solution of PVA/H_3PO_4.

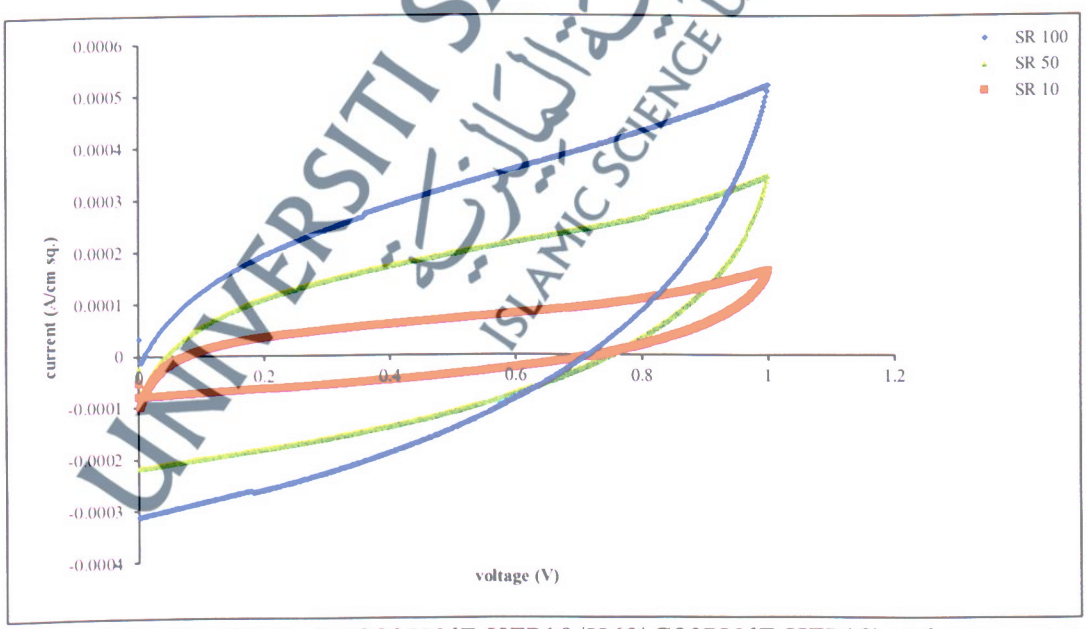

Figure 4.12 CV of Cell –B (C90PVdF-HFP10 |H60| C90PVdF-HFP10) at the scan rates of 10, 50 and 100 mV.

Table 4.8 CV Performances of cell- B (C90PVdF-HFP10 |H60| C90PVdF-HFP10)

Cell	Working voltage (V)	Capacitance value of different scan rates (Fg^{-1})		
		100 mV	50 mV	10 mV
B-C90H60	1	16	19	23

Last but not the least, in this category of CPCMWCNTs is the CV of Cell –C (C90PVdF-HFP10 |H70| C90PVdF-HFP10) at the scan rates of 10, 50 and 100 mV for a voltage window of 0.0 – 1.0 V displayed in Fig. 4.13. This is best performed cell, as it can be noticed from Table 4.9, the capacitance delivery increased dramatically to 94, 172 and 313 Fg^{-1} for the same scan rates of 100, 50 and 10 mV respectively. It can also be discerned that, the resulting CV curves of this cell displayed a better leaf-like and mirror symmetric which indicate an ideal supercapacitive behavior for CPCMWCNTs in an aqueous electrolyte of 70 wt.% of H_3PO_4 in homogenous solution of PVA/H_3PO_4.

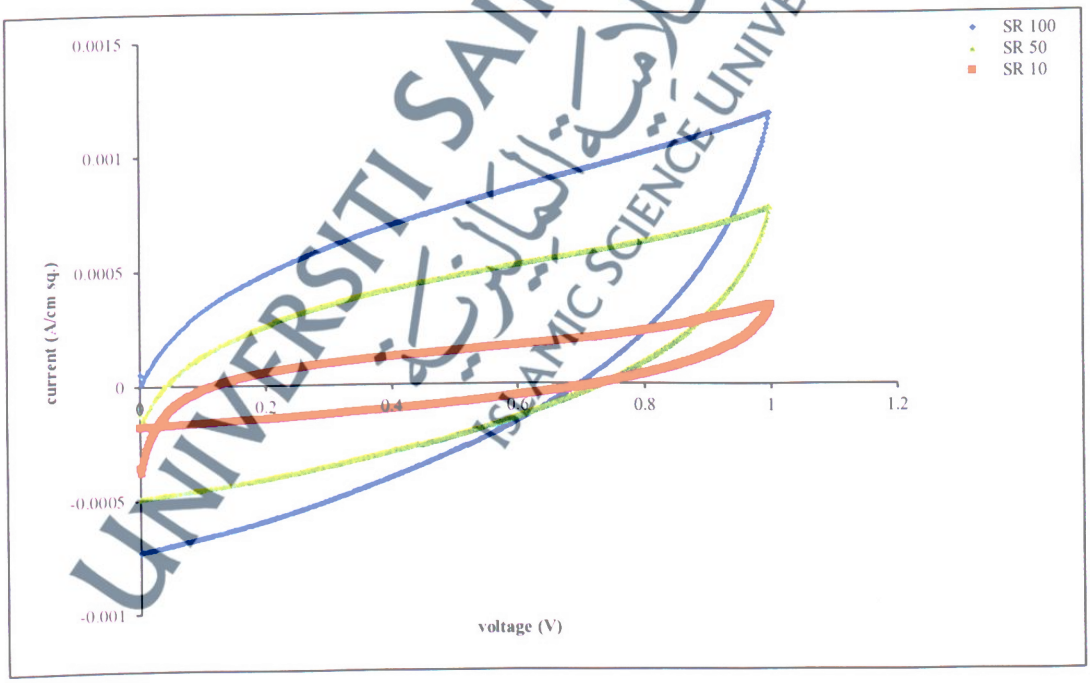

Figure 4.13 CV of Cell –C (C90PVdF-HFP10 |H70| C90PVdF-HFP10) at the scan rates of 10, 50 and 100 mV.

Table 4.9 CV Performances of Cell –C (C90PVdF-HFP10 |H70| C90PVdF-HFP10)

Cell	Working voltage (V)	Capacitance value of different scan rates (Fg^{-1})		
		100 mV	50 mV	10 mV
C-C90H70	1	94	174	313

At this juncture, it should be reminded that, the amount of electrical charge accumulated due to electrostatic attraction in supercapacitor depends on the area of the electrode/electrolyte interface that can be accessed by the charge carriers. Once the area can be accessed fully by the charge carriers, then the higher surface area of the electrode material the higher capacitance. However, this is not always the case for all supercapacitor cells as the higher surface area does not always result in higher capacitance because the capacitance also depends on the pore size, the size distribution and conductivity of both the electrolyte and the active materials (Pan et al. 2010). Therefore, higher capacitance can be achieved by optimizing all of the related factors. It has been clearly mentioned in the methodology that this commercially obtained CNTs is a functionalized one, has an outer diameter of >50nm and a moderate surface area of 43 m^2g^{-1}. Delivering different values of capacitance at different cell formations (as in cells A, B and C) shows the conductivity of the electrolyte has affected the performance of the supercapacitor significantly. For example, Pan et al. (2010) has reported a vertically aligned CNTs with the diameter of about 25 nm and a specific area of 69.5 m^2g^{-1} with a specific capacitance of just 14.1 Fg^{-1} and portrayed an excellent rate capability.

One of the criteria in supercapacitor's fabrication and application is its ability to endure long term cycling stability. In this respect, the cycling endurance measurement over 5000 cycles for the cell A (as shown in Fig. 4.14) was conducted using the CD test

at the working voltage of 1 V. The figure displayed the graph of resulting capacitance as a function of cycling number. It can be seen from the graph that, the cell exhibits the best cycling stability with only about 50 % capacitance retention of its initial value after 5000 cycles. Earlier discussions reveal possible factors that hinder the performance of this cell. Major contributing factor is the low conductivity of the electrolyte (H50) used during the cell fabrication.

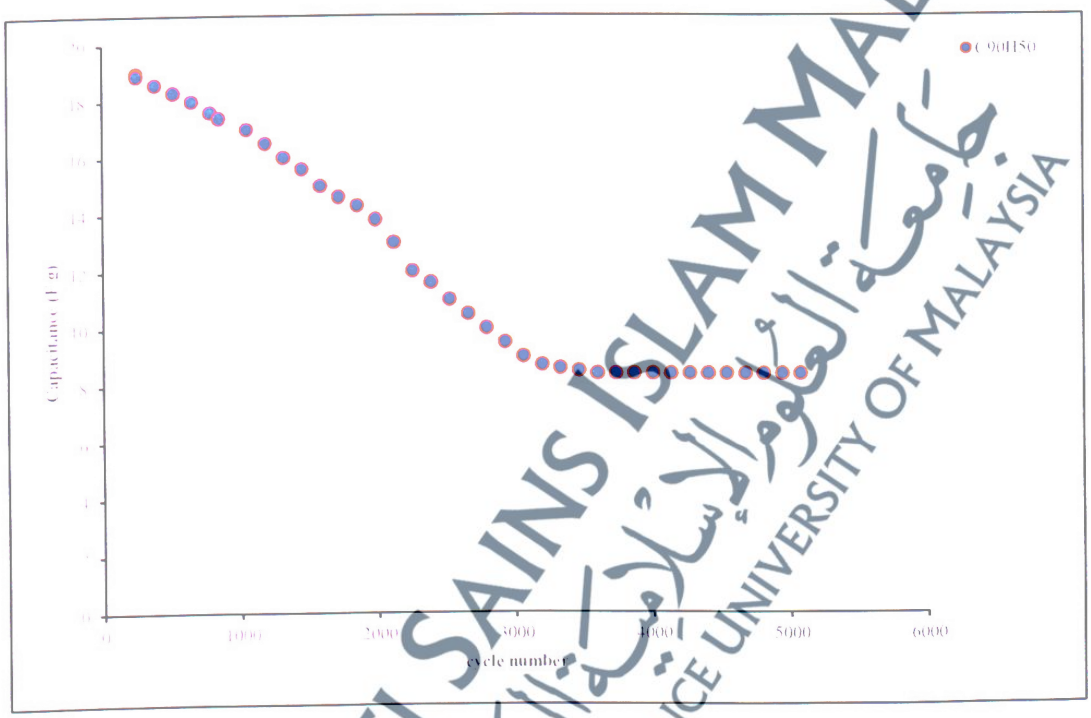

Figure 4.14 Cyclic performances of cell-A (C90PVdF-HFP10 |H50| C90PVdF-HFP10) for a working voltage of 1 V.

Furthermore, Fig. 4.15 displayed the cycling endurance measurement over 5000 cycles for the cell – B which was carried out using the CD test at the working voltage of 1 V. Of note, compared to cell – A and as shown from the figure, cell – B which has higher capacitance over cell showcased the best cycling stability with about 85 % capacitance retention of its initial value after 5000 cycles. As mentioned earlier, and proved by the capacitance value of this cell, increase in conductivity of the electrolyte compared to cell – A could be the contributing factor for its cycling stability as well.

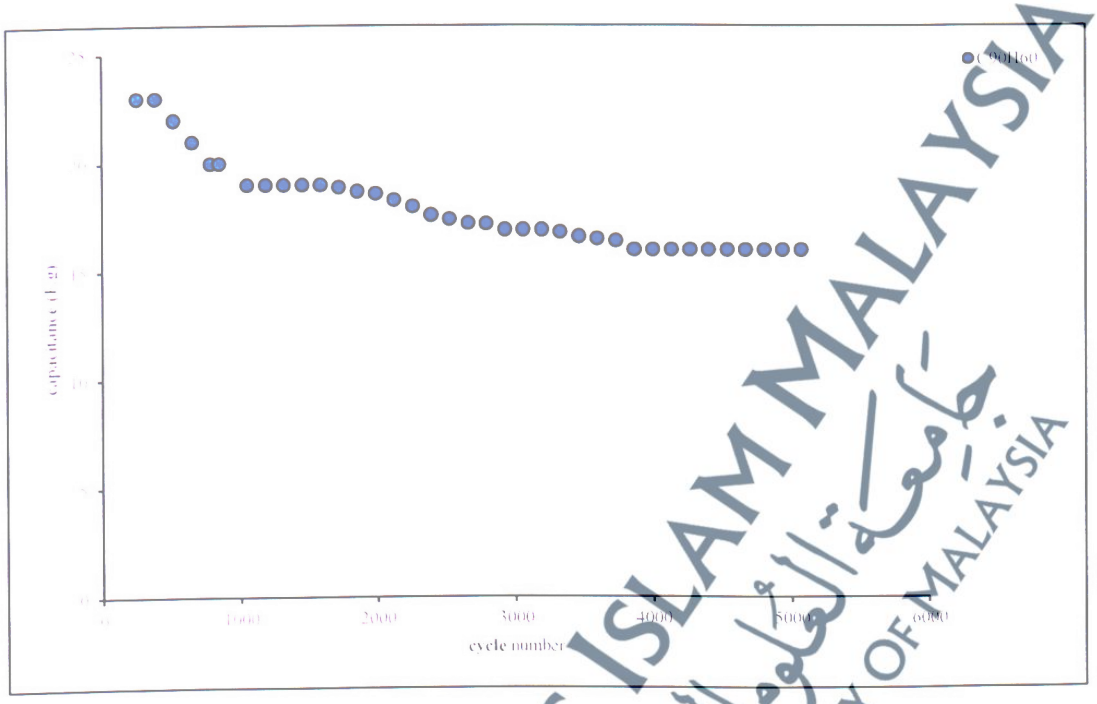

Figure 4.15 Cyclic performances of cell-B (C90PVdF-HFP10 |H60| C90PVdF-HFP10) for a working voltage of 1 V.

Moreover, Fig. 4.16 displayed the cycling endurance measurement over 5000 cycles for the cell – C carried out using the CD test at the working voltage of 1 V. Unlike cell – A and B, cell – C although, displayed about 58 % capacitance retention of its initial value, however, the capacitance value even at this level (~ 184 Fg^{-1}) is quite promising. It was elaborated earlier that although all the three aforementioned cells were made from carboxyl CNT and shared common characteristics in terms of outer diameter and surface area. The separators (H50, H60 and H70) used have considered the major contributing factors to their differences in conductivities.

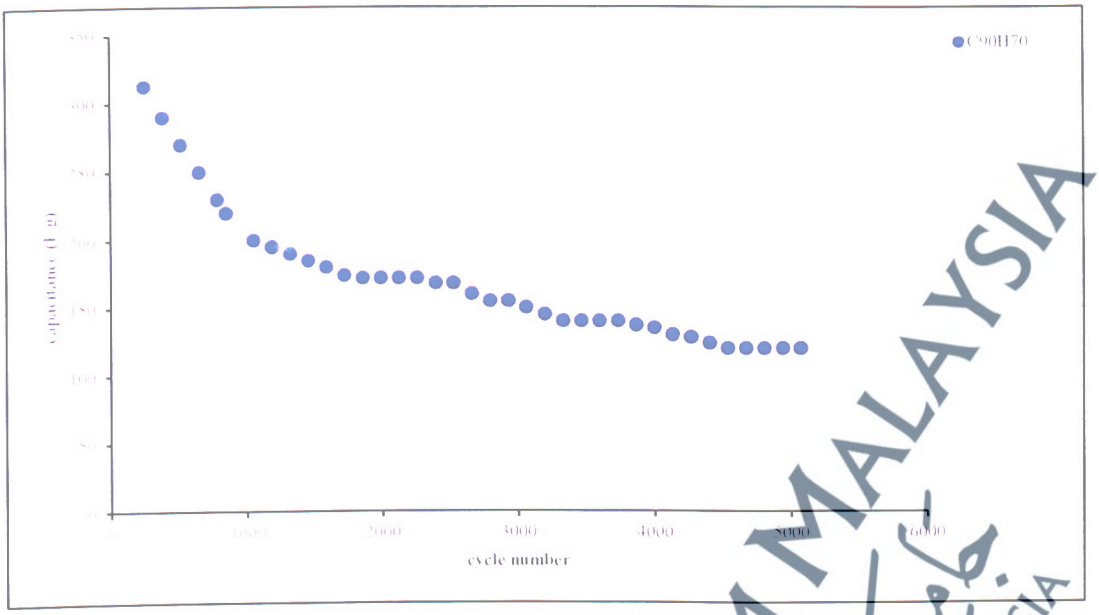

Figure 4.16 Cyclic performances of cell-C (C90PVdF-HFP10 |H70| C90PVdF-HFP10) for a working voltage of 1 V.

Galvanostatic CD is the accepted measurement method for determining capacitance for packaged supercapacitor in the supercapacitor industry and correlates more closely to how a load is typically applied to such supercapacitor in the majority of applications. Most importantly the same voltage range should be used for testing should match that used for commercial cells and should reflect the electrolyte's electrochemical window. For instance, an electrochemical window from 0.0 V to approximately 1.0 V, should be used for aqueous electrolytes and 0.0 V to 2.5–2.7 V for organic electrolytes. This is because, driving a cell above its true maximum operating voltage can lead to an overestimation of specific capacitance and cells operated at these levels will have shortened lifetimes and poor efficiencies due to the non-reversible reactions within the cell. Significant errors can also be introduced by the method used to calculate the slope (DV/dt) (Stoller & Ruoff, 2010). In a theoretical sense, for a constant capacitor device with less effect on high internal resistance, the constant-current charge and discharge relations are straight lines with +1/c and -1/c respectively (Niu et al., 2006). In this respect, we determined the capacitance of the supercapacitor cell yet using this method.

Furthermore, Fig. 4.17, the CD graphs of (a) Cell-A (b) Cell-B and (c) Cell- C were all depicted at a working voltage of 1.0 V and at three different discharge current (i.e. 10, 20 and 100 mA). The discharge capacitance was calculated from the equation 3.5 mentioned in the methodology chapter.

In Fig.4.17 (a) a typical CD profile of cell – A that is made up of an electrode from CPCMWCNTs of the average porous surface area of about 43 m^2g^{-1} and an aqueous hybrid polymer electrolyte of 50 wt.% of the H_3PO_4 of the overall PVA/H_3PO_4 blends (H50) is shown. A voltage range of 0.0 – 1. 0 V was used in order to ascertain the significance of the cell at higher voltage. It can be seen that the CD profiles deviate from a typical linear variation of voltage with time that is known for a supercapacitor. The observed non-linearity in this case can be attributed to the low conductivity of the electrolyte. It can also be observed that the charging and discharging times are almost the same. The specific capacitance of 1.4, 3.5 and 10.5 Fg^{-1} are obtained at a discharge current of 100, 20 and 10 mA respectively, with a specific energy and power densities of 5.25 Whg^{-1} and 0.08 Wg^{-1} respectively, at a discharge current of 100 mA. The overall columbic efficiency of 88.9 % is recorded for this cell. Table 4.10 summarizes all the aforementioned results. There is a large voltage drop at the beginning of the discharge curve which could be as a result of the porous nature of the electrode and low conductivity of the electrolyte. It could be recalled in our earlier discussion that the porosity of the electrode can sometimes influence the performance of the supercapacitor. This electrode being ~50 nm in outer diameter can hence be an attributing factor towards its cell's voltage drop.

Furthermore, Fig. 4.17 (b) shows a CD profile of cell – B, which has an electrolyte of better conductivity compared to cell – A (i.e. H60). Although, the

variation of voltage with respect to time is again not linear due to the porous nature of the electrode materials which is in conformity with the argument put by Pan et al. (2010), the profile, however, is more perfect than that of cell – A. This could be as a result of improvement in the conductivity of the electrolyte. Moreso, the reduction of ERS can be attributed to the improvement in conductivity because of the carrier induced by the functionalization (Pan et al., 2010). It's charging and discharging times are observed to be the same, and the specific capacitance of 2.4, 6.0 and 18.0 Fg^{-1} are obtained at discharge current of 100, 20 and 10 mA respectively, with a specific energy and power densities of 5.25 Whg^{-1} and 0.08 Wg^{-1} respectively, at a discharge current of 100 mA. Its overall columbic efficiency of 88.9 % is recorded (Table 4.10). However, the voltage drop noticed at the beginning of the discharge curve is not as large as that of cell – A which could be as a result of improvement in the conductivity of the electrolyte.

Unlike cells – A and B, which shows their CD profile with non-linearity and a large voltage drop, Fig 4.17 (c) shows perfect linear characteristic implying a formation of good electrode/electrolyte interface with a well-defined conductivity. In addition, no ohmic drop is observed in this case. We have employed three different discharge currents for the measurement as mentioned earlier. Again, it can also be observed that the charging and discharging times are almost the same. The specific capacitance of 20.3, 51.2 and 153.0 Fg^{-1} are obtained at discharge current of 100, 20 and 10 mA respectively, and a specific energy and power densities of 76.50 Whg^{-1} and 1.00 Wg^{-1} respectively, at the said discharge current of 100 are also calculated. The overall columbic efficiency of 93.8 % is recorded for this cell. The introduction of surface carboxyl groups can create more than 3 times larger capacitance due to the increased

hydrophilicity of MWCNTs in an aqueous electrolyte. This is not always the same case for the introduction of alkyl groups, as it will result in a marked decrease in capacitance. Overall, it can be observed from all the cells that, the discharged capacitance decreases with the increase in the current applied, which could be as a result of the low penetration of ions into the inner region of the pores due to fast potential changes.

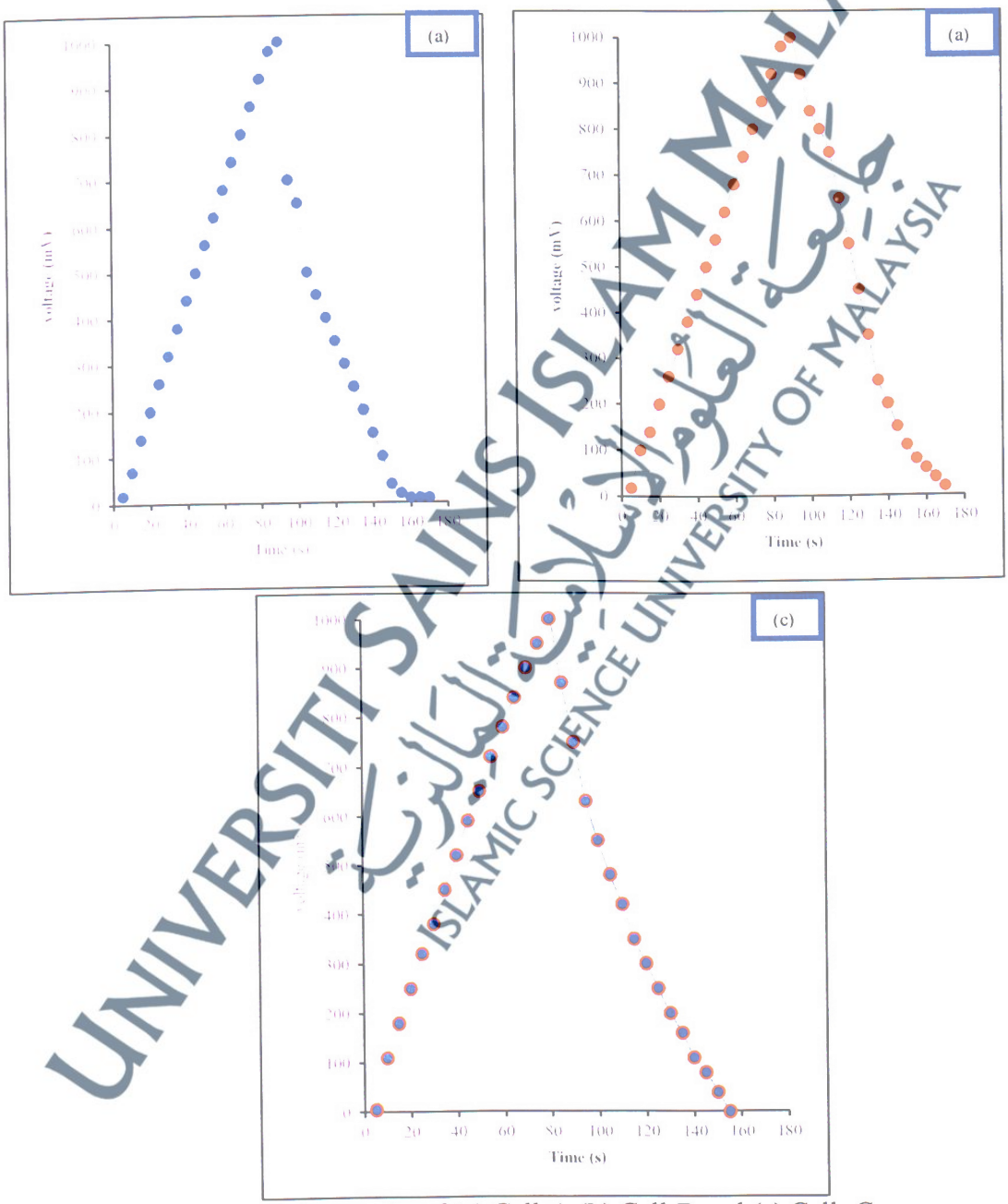

Figure 4.17 CD graphs of **(a)** Cell-A **(b)** Cell-B and **(c)** Cell- C.

Table 4.10 Performance of Supercapacitor by the CD

Cells	Working voltage (V)	C_d (Fg^{-1})	Energy density (Whg^{-1})	Power density (Wg^{-1})	Efficiency (%)
A-C90H50	1	1.4-3.5	5.25	0.08	88.9
B-C90H60	1	2.4-18.0	9.00	0.50	88.9
C-C90H70	1	20.3-153.0	76.50	1.00	93.8

So far from the foregoing section, the noble of CPCMWCNT used as an electrode for high performance supercapacitors using HPSE as a separator have been explored. Three cells were constructed and labeled as cell-A (C90PVdF-HFP10 |H50| C90PVdF-HFP10), cell-B (C90PVdF-HFP10 |H60| C90PVdF-HFP10) and cell-C (C90PVdF-HFP10 |H70| C90PVdF-HFP10) with changes in the separator. The XRD peaks of the sample electrode C90PVdF-HFP10 appeared in $2\theta = 26^0$ and $2\theta = 43^0$ which might be as a result of the hexagonal structure of (002) and (101) respectively, which also indicates that the carboxyl Multiwalled CNTs have high conductivity and can be used as an electrode material for the fabrication of the supercapacitor cell. Again, a wider diffraction at $2\theta = 20.1^0$ which correspond to crystalline peaks of PVDF. TGA traces shows that, the pure CPCWMCNT experience a major loss of just 11.1 %, which occurred at 611.8 ^{0}C leaving a residue of 87.9 %, which also shows that, the pure MWCNT have very good thermal stability and consequently, good in application for electrochemical devices. This result, even gets better when the active material was added. From the overall results for the electrochemical analysis of the CV, cell – C delivered highest capacitance of 313 Fg^{-1} by more than 3 folds over cells A and B. This result, as mentioned earlier, is attributed to the remarkable increase in conductivity of the electrolyte used (H70) which has the highest conductivity over H50 and H60 used in the assembly of cell A and B respectively. This was further proved by the CD

analysis where cell – C shows perfect linear characteristic implying a formation of good electrode/electrolyte interface with a well-defined conductivity. In addition, no ohmic drop is observed in the profile delivering the highest specific capacitance of 153.00 Fg^{-1} and a specific energy and power densities of 76.50 Whg^{-1} and 1.00 Wg^{-1} respectively, and attained the overall columbic efficiency of 93.8 %. In the next section, fabrication of supercapacitor using yet another functionalized carbon nanotube (CPHMWCNTs) will be explored. Several test analyses will also be conducted and final capacitance, power and energy densities will be analyzed.

4.3 Fabrication and Characterizations of Supercapacitor Based on the Commercially Prepared Hydroxyl Multiwalled Carbon Nanotubes (CPHMWCNTs) and Hybrid Solid Polymer Electrolytes (HSPE)

4.3.1 Microstructure Characterizations

The XRD analysis of the H90PVdF-HFP10 electrode is depicted in Fig. 4.18. It can be seen that, all diffraction peaks can be observed and the major diffraction peaks of the CPHMWCNT can also be seen clearly. The first two points, peaks that appeared at $2\theta = 26^0$ and 43^0 which matched with (002) and (101) respectively that the presence of MWCNT, while the last point on the right side, i.e. $2\theta = 56.1^0$ (also red vertical lines) might be also considered part of the commercial CNT.

The intensity of the peak also can be to have high conductivity (Dong et al., 2007) of the as-prepared carbon electrode. Furthermore, diffraction peak at $2\theta = 20.1^0$ (the blue vertical line), at the beginning left of the trace, which correspond to the crystalline peaks of the PVDF (Stolarska et al., 2007). Similar XRD results were obtained by (Stolarska et al., 2007; Li et al., 2010b). The dispersed green vertical lines all over the trace are attributed to the functionalization of the CNT (-COOH).

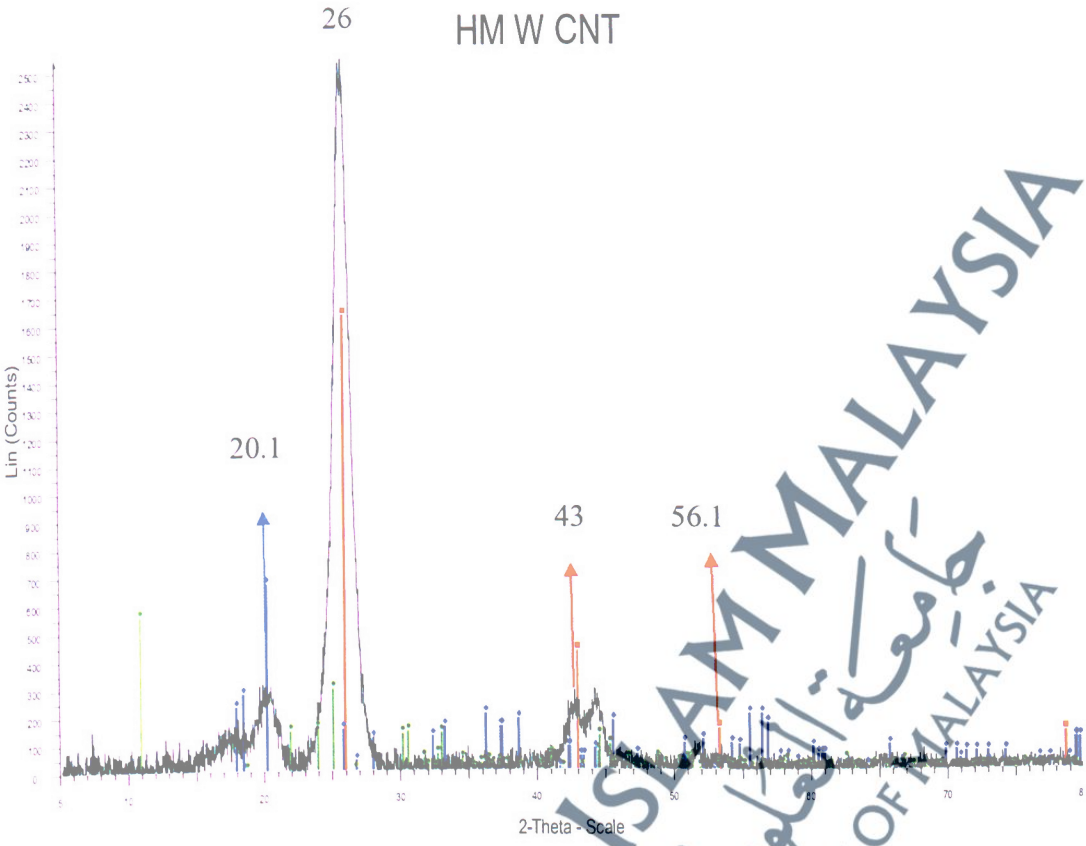

Figure 4.18 XRD plot of CPHMWCNTs with red, green and blue vertical lines. The red vertical lines indicate the presence of CNT, green detects the presence of -COOH while blue indicating the presence of PVdF.

As for the FESEM analysis, Fig. 4.19 (a) and (b), FESEM images of CPHMWCNTs of pure CPHMWNTs and sample electrode with 90 % CPHMWNTs were respectively presented. In this case, both the two samples exhibit similar regular, entangled and smooth surface morphology with the outer diameter of ~28 nm and length of several micrometers. Although, few larger tubes can be seen in the FESEM structure which indicate that the original MWCNT has been functionalized since the normal outer diameter does not exceed 50 nm. In terms of clarity, sample in Fig. 4.19 (a) shows clarity of sample (b) due to the addition of 10 wt.% of the binder.

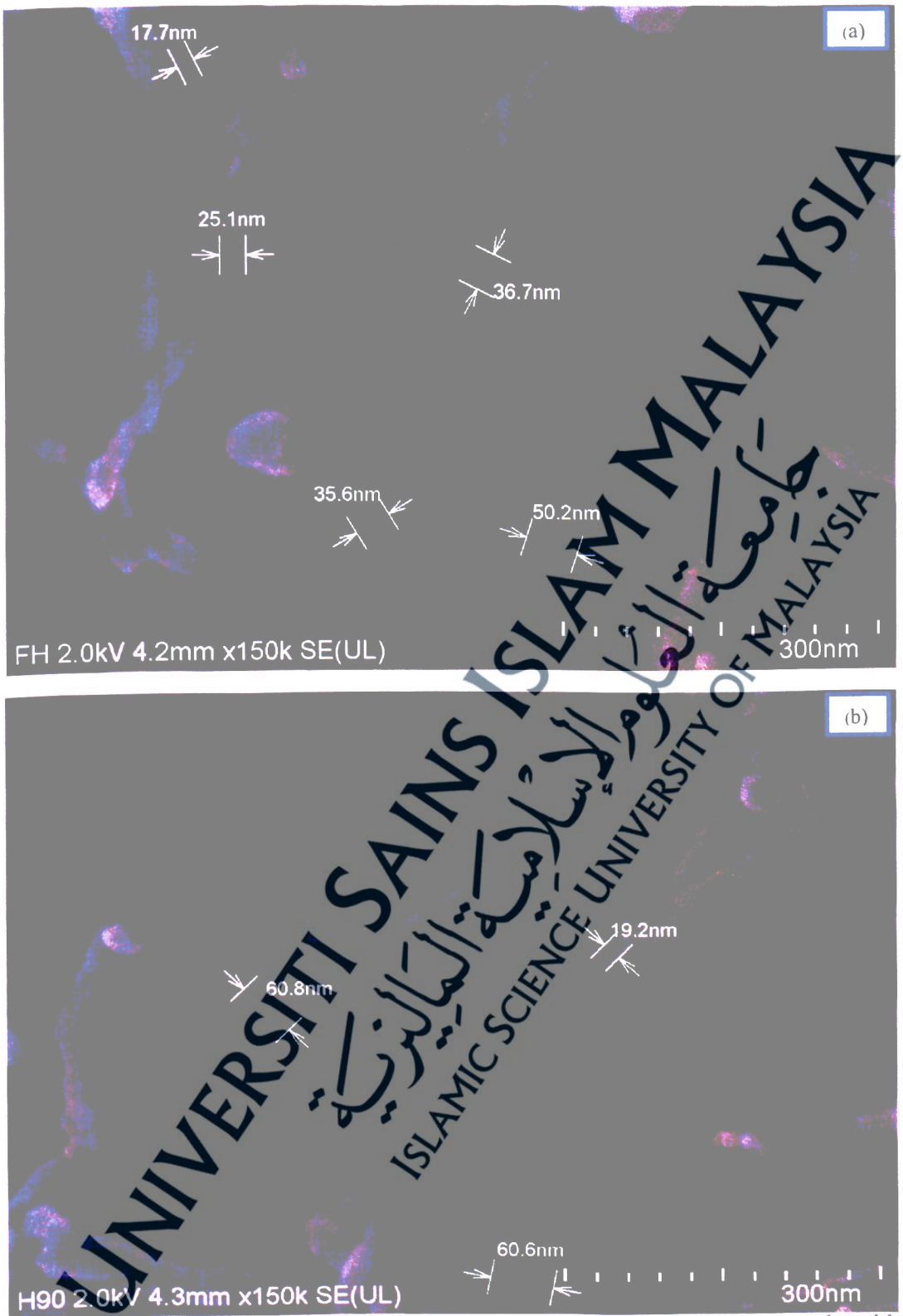

Figure 4.19 FESEM images of **(a)** pure (free) CPHMWCNTs and **(b)** sample with 90 wt.% of CPHMWNTs showing the average outer diameters of the tubes. The magnifications of the two samples were 4.2 mm x 150 k and 4.3 mm x 150 k respectively.

Moreover, Fig. 4.20 depicts the FESEM images of H80PVdF-HFP20 electrode overlapped on hybrid electrolyte containing 60 wt.% of the H_3PO_4 (H60) at the magnifications of 2.0 kV x 100 k (500 nm). This image was also taken at an angle of 30^0 in order to examine the edge contact at the electrode and electrolyte. As mentioned earlier the reason behind the image taken is to deduce the required needed during the sandwiching of the electrolytes between the electrolytes to avoid high resistance and consequent low conductivity of the assembled cell.

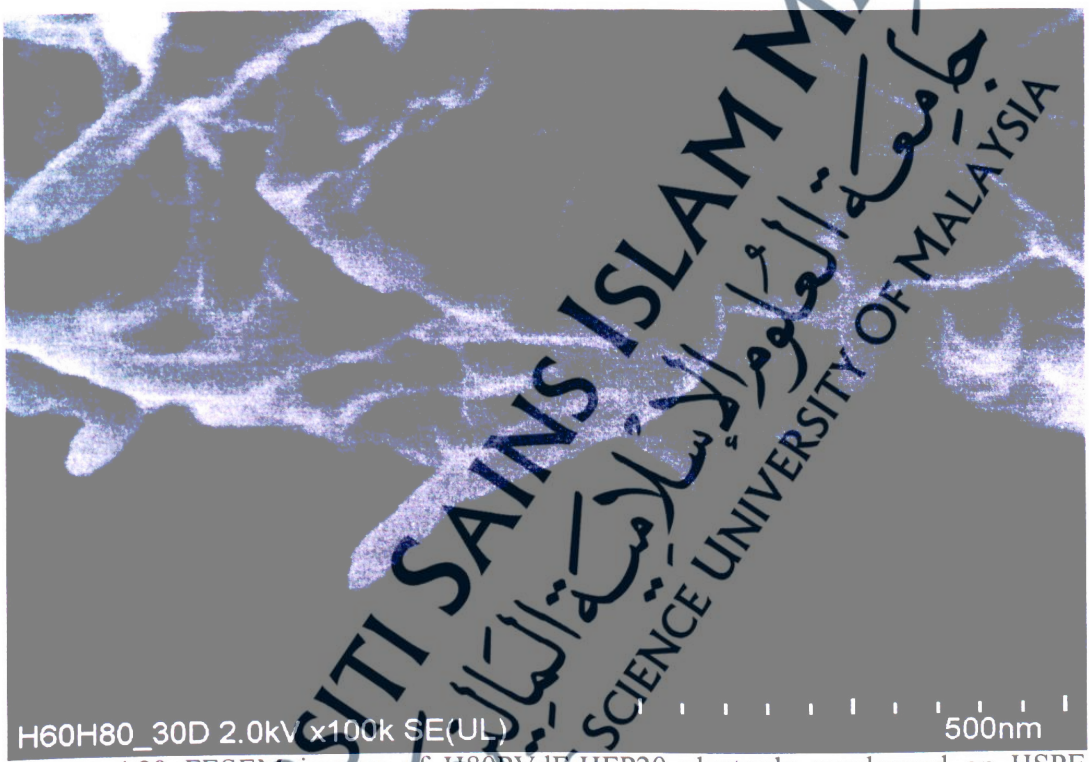

Figure 4.20 FESEM images of H80PVdF-HFP20 electrode overlapped on HSPE containing 60 wt.% of H_3PO_4, 80 wt.% of CPHMWCNTs at the magnification of 2.0 kV x 100 k (500 nm) and an angle of 30^0.

4.3.2 Thermogravimetric Analysis (TGA)

It has been stated earlier that, the analysis of the temperature stability of the sample was investigated by thermal analyzer in the scale-range of 50 ^{0}C to 1000 ^{0}C under nitrogen gas (N_2) flow at a heating rate of 10 ^{0}C min^{-1} on a METTLER, STAR^e SW 10.00. The thermal stability of the samples was discerned in Fig. 4.21. These figure include (a) 0

% sample (Background) (b) pure CPHMWCNT (c) H90PVdF-HFP10 – Single scale (d) H90PVdF-HFP10 – Double scale.

At the beginning, we analyzed background heating, in order to make way with any ruminant residue and for re-standardization. From the trace in Fig. (b), it can be understood that, the pure HPCWMCNT with major loss of merely 10.1 % occurring at 696.6 ^{0}C leaving a balance of 88.7 %. Basically, these results show that pure MWCNTs has very good thermal stability and consequently, good in application of electrochemical devices. While in Fig. 4.21 (b) and (c), it can be noticed that, when the active materials (i.e. the binder) was added into a single electrode, three losses were recorded. The initial loss of 0.9 % of the total samples occurs at 274.7 ^{0}C, then the second loss of 4.1 % occurred at 388.9 ^{0}C and the highest loss of 7.1 % was noticed at 605.4 ^{0}C. This shows that incorporating a binder (of negligible quantity) into the pure CPHMWCNTs does not affect the conductivity supercapacitor.

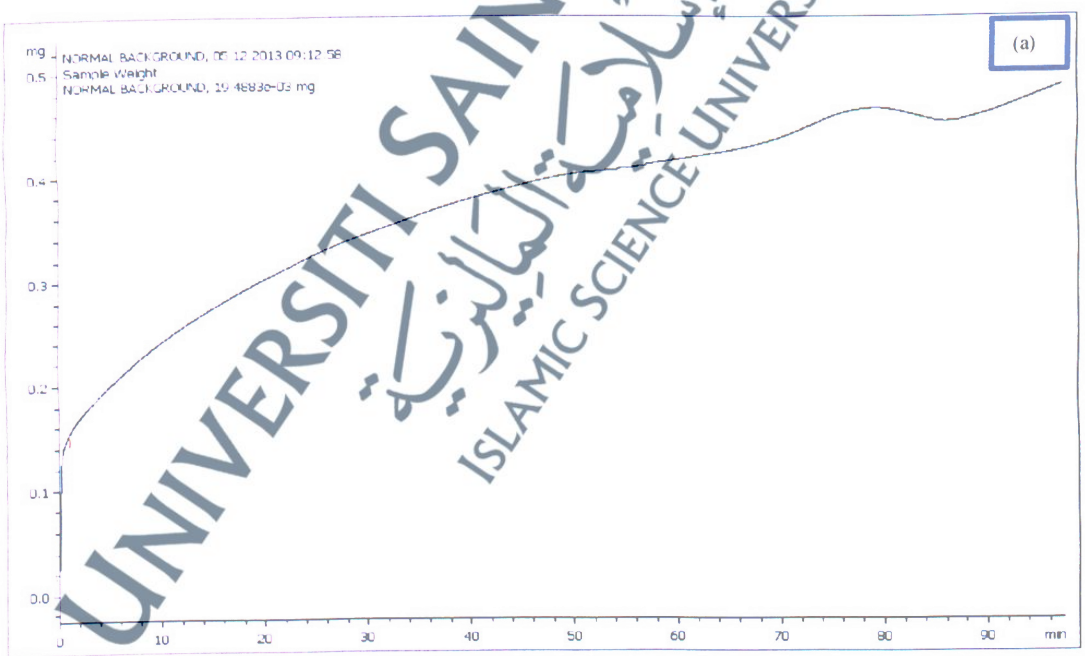

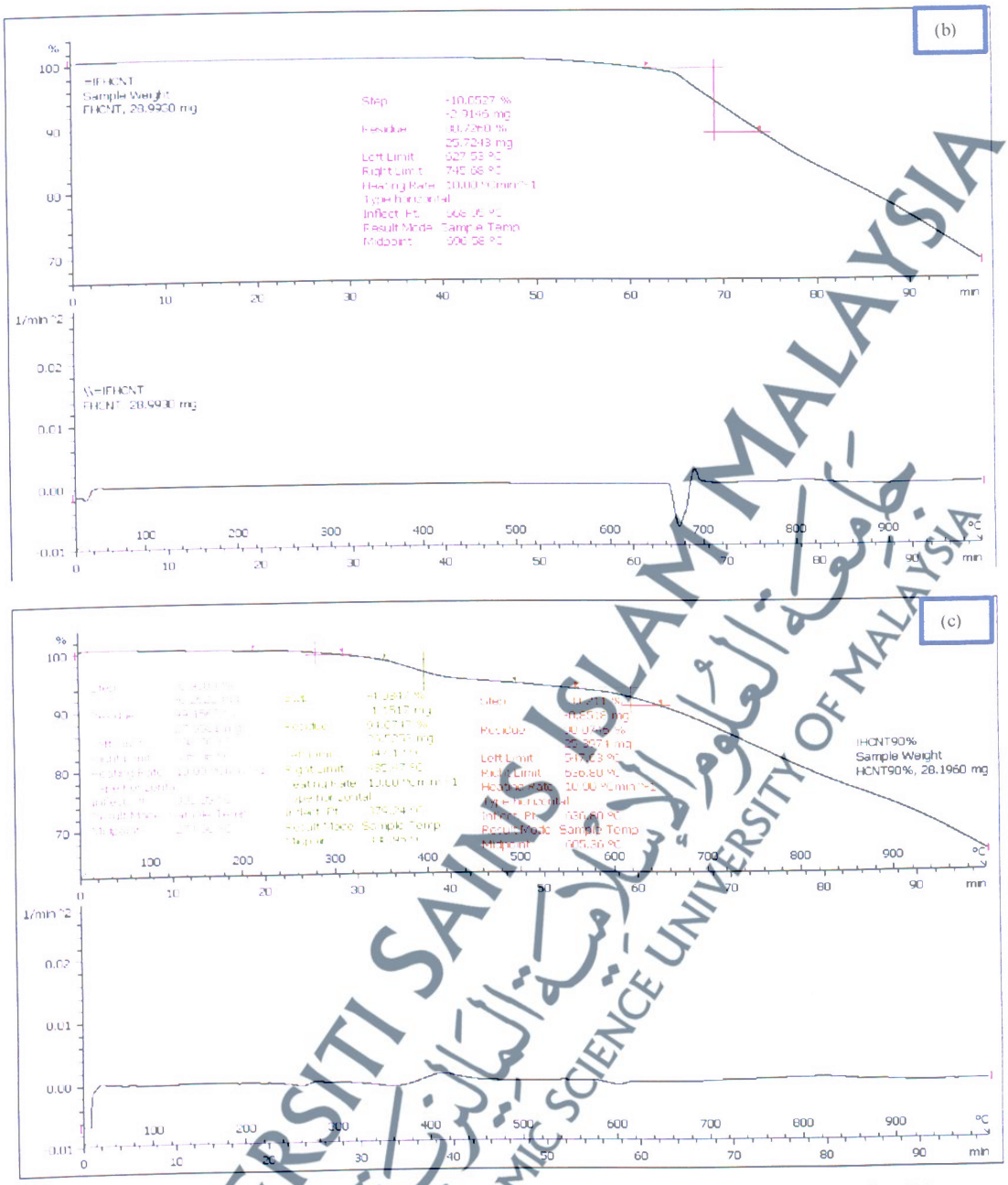

Figure 4.21 TGA of the electrode at **(a)** 0 % sample (Background) **(b)** pure CPHMWCNT **(c)**: H90PVdF-HFP10 – Double scale.

4.3.3 Electrochemical Behavior

Earlier, it was reported that, of the eight different formations of the polymer electrolytes using cellulose filter incorporated in an aqueous electrolyte, which were prepared in a percentage ratio from 0 – 70 wt.% of PVA/H_3PO_4 blends three, with the highest

electrical conductivity are selected for the fabrication of the supercapacitor cell. They are the samples with 50, 60 and 70 wt.% of the orthophosphoric acid, which also coded as H50, H60 and H70 respectively. The electrochemical behaviors of the cells constructed from sandwiching the electrode and electrolyte using two-electrode system is therefore investigated by CV and CD measurements.

CVs are performed to estimate the electrochemical properties of the symmetric supercapacitors in these three different electrolytes at the scan rate of 10, 50 and 100 mV with the voltage range from 0.0 – 1.0 V. The results for the cell – A (H90PVdF-HFP10 |H50| H90PVdF-HFP10) are shown in Fig. 4.22. It can be found that the supercapacitors in their voltage range exhibit similar leaf-like (although known rectangular) and mirror symmetrical modest capacitive behavior, with slow current responses on voltage reversal at the two end potentials. It might be inherent to the nature of electrolyte used (i.e. H50, which has the lowest conductivity among the selected electrolytes).

From the calculation, it could be obtained that the specific capacitance is 18, 22 and 46 Fg^{-1} for scan rates of 100, 50 and 10 mV, respectively as shown in Table 4.11. From these results it can be deduced that, there is the relationship between the capacitance and scan rate. The specific capacitance decreases from 46 Fg^{-1} to 18 Fg^{-1} which could be attributed to the slow transfer of ions on the electrode electrolyte interface (Shu et al., 2013). It is also important to note that, the lower conductivity of the electrolyte film can lead to lower capacitance. The film H50, which was used as a separator has the conductivity of 8.64×10^{-5} Scm^{-1}, this is another evidence for the resulted low capacitance of the cell.

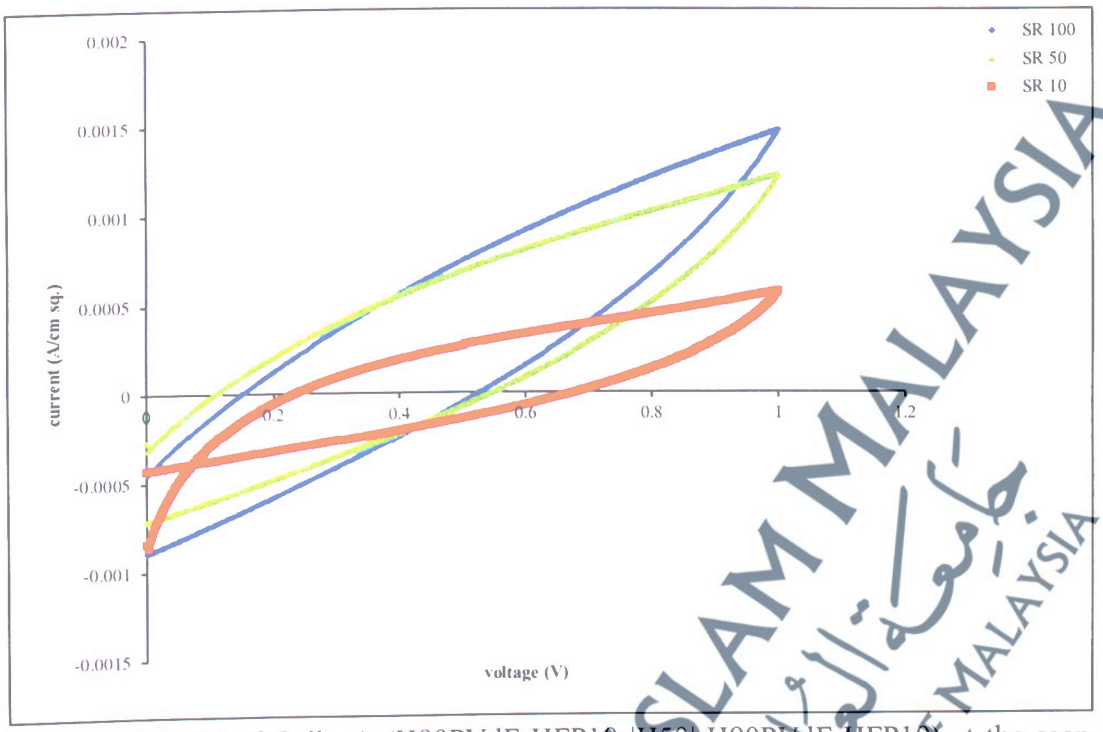

Figure 4.22 CV of Cell A (H90PVdF-HFP10 |H50| H90PVdF-HFP10) at the scan rates of 10, 50 and 100 mV.

Table 4.11 CV Performances of Cell –A (H90PVdF-HFP10 |H50| H90PVdF-HFP10)

Cell	Working voltage (V)	Capacitance value of different scan rates (Fg^{-1})		
		100 mV	50 mV	10 mV
A-H90H50	1	18	22	46

Furthermore, Fig. 4.23 also shows CV of Cell–B (H90PVdF-HFP10 |H60| H90PVdF-HFP10) at the scan rates of 10, 50 and 100 mV for a voltage window of 0.0 – 1.0 V. Noting from this cell, the electrolyte used in this cell (H60), its specific capacitances improved remarkably to 48, 56 and 89 Fg^{-1} for scan rates of 100, 50 and 10 mV respectively (see Table 4.12). These results almost double that of cell-A by two folds which might be attributed to the increase in ionic conductivity in the polymer electrolyte of the HSPE. Unlike the curves of cell A, the resulting CV curves of this cell

displayed a better leaf-like and mirror symmetric indicating an ideal supercapacitive behavior for CPHMWCNTs that uses an aqueous electrolyte of 60 wt.% of H_3PO_4 in homogenous solution of PVA/H_3PO_4.

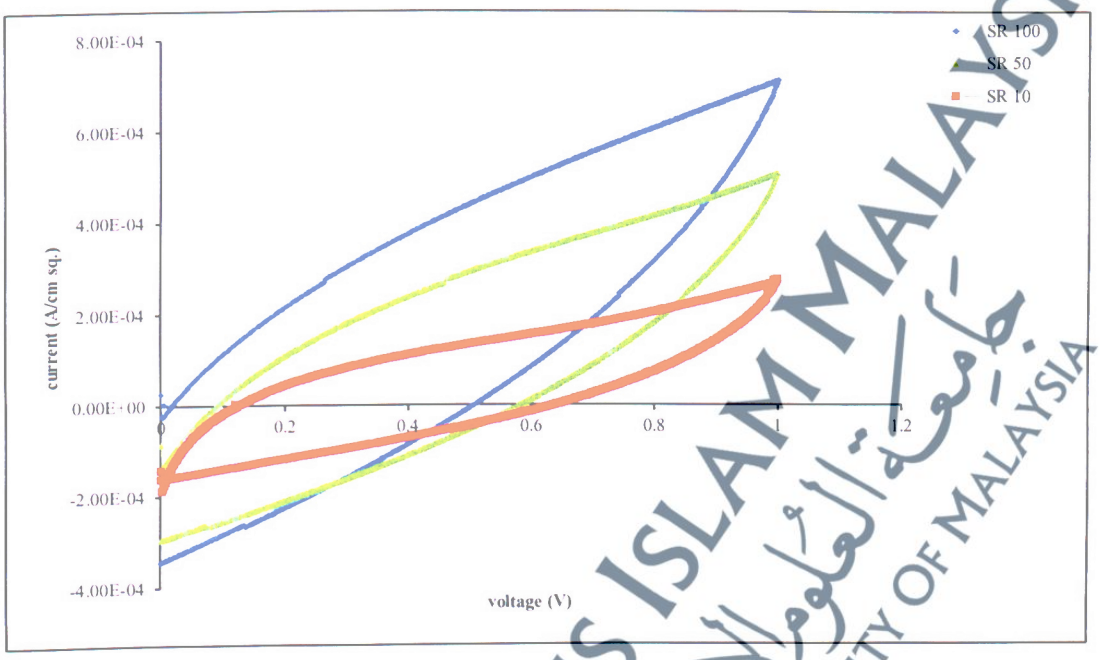

Figure 4.23 CV of Cell –B (H90PVdF-HFP10 |H60| H90PVdF-HFP10) at the scan rates of 10, 50 and 100 mV.

Table 4.12 CV Performances of cell- B (H90PVdF-HFP10 |H60| H90PVdF-HFP10)

Cell	Working voltage (V)	Capacitance value of different scan rates (Fg^{-1})		
		100 mV	50 mV	10 mV
B-H90H60	1	48	56	89

Last but not the least, in this category of CPHMWCNTs is the CV of Cell –C (H90PVdF-HFP10 |H70| H90PVdF-HFP10) at the scan rates of 10, 50 and 100 mV for a voltage window of 0.0 – 1.0 V displayed in Fig. 4.24. This is best performed cell, as it can be noticed from Table 4.13, the capacitance delivery increased dramatically to 52, 62 and 92 Fg^{-1} for the same scan rates of 100, 50 and 10 mV respectively. It can also be discerned that the resulting CV curves of this cell displayed a better leaf-like

and mirror symmetric which indicate an ideal supercapacitive behavior for a CPHMWCNTs in an aqueous electrolyte of 70 wt. % of H_3PO_4 in homogenous solution of PVA/H_3PO_4.

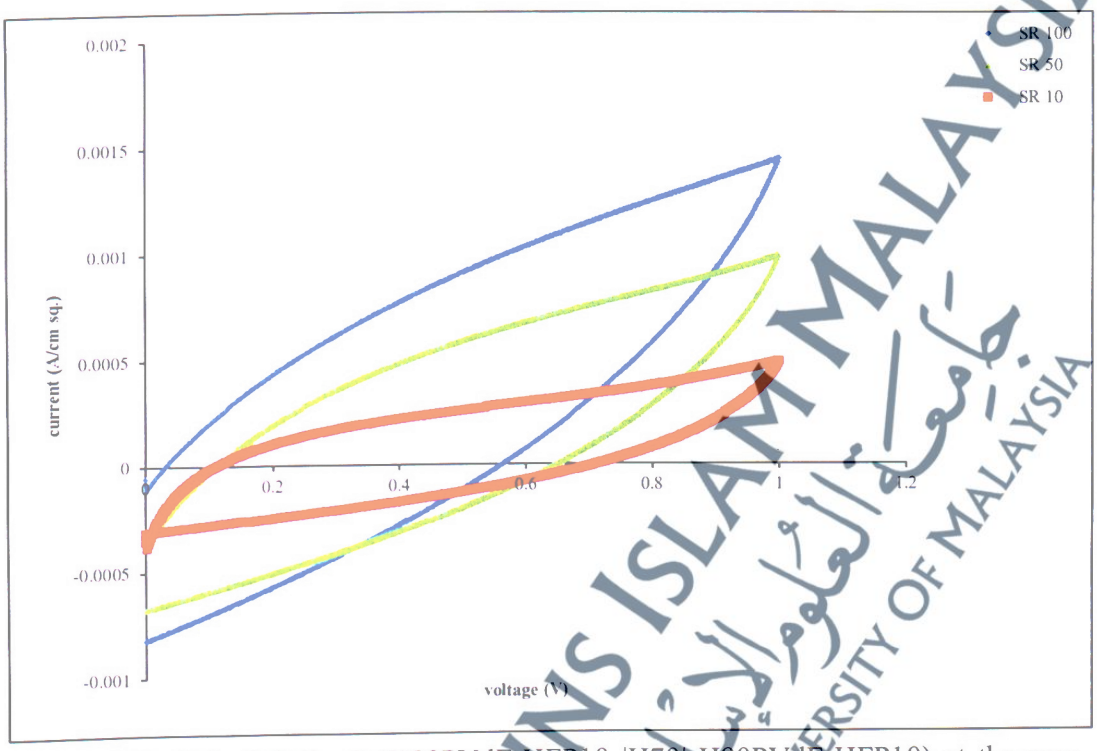

Figure 4.24 CV of Cell –C (H90PVdF-HFP10 |H70| H90PVdF-HFP10) at the scan rates of 10, 50 and 100 mV.

Table 4.13 CV Performances of Cell –C (H90PVdF-HFP10 |H70| H90PVdF-HFP10)

Cell	Working voltage (V)	Capacitance value of different scan rates (Fg^{-1})		
		100 mV	50 mV	10 mV
C-H90H70	1	52	62	92

The observed differences of the CV behaviors for the supercapacitors in various electrolytes of the aforementioned three cells (cells A, B and C) could be attributed to, the ionic radius of the electrolytes, the radius of ionic hydration sphere of electrolytes, the conductivity of the ions and the mobility of the ions. It is a known fact that, the ions would be surrounded by the water of hydration when the water is used as the solvent.

Thus, the electric double layers will be built by the ionic hydration sphere of electrolytes (Zhang et al., 2012).

It is of utmost importance to mention here that, one of the criteria in supercapacitor's fabrication and application is its ability to endure long term cycling stability. In this light, the cycling endurance measurement over 5000 cycles for the cell A (as shown in Fig. 4.25) was conducted using the CD test at the working voltage of 1.0 V. The figure displayed the graph of resulting capacitance as a function of cycling number. It can be seen from the graph that, the cell exhibits the best cycling stability with only about 42 % capacitance retention of its initial value after 5000 cycles. It was earlier revealed that possible factors that hinders the performance of this cell could lower conductivity of the electrolyte (H50) used during the cell fabrication.

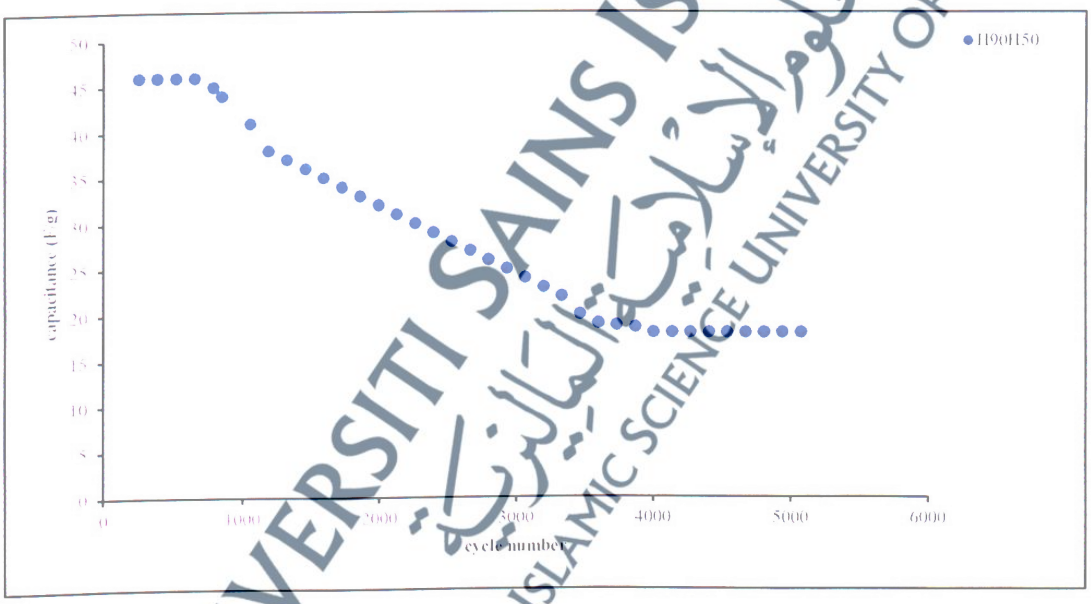

Figure 4.25 Cyclic performances of cell-A (H90PVdF-HFP10 |H50| H90PVdF-HFP10) for a working voltage of 1 V.

Furthermore, Fig. 4.26 displayed the cycling endurance measurement over 5000 cycles for the cell B which was carried out using the CD test at the working voltage of 1 V. Of note, compared to cell A and as shown from the figure, cell B which has higher

capacitance over cell showcased the best cycling stability with about 60 % capacitance retention of its initial value after 5000 cycles. As mentioned earlier, and proved by the capacitance value of this cell, increase in conductivity of the electrolyte compared to cell A could be the contributing factor for its cycling stability as well.

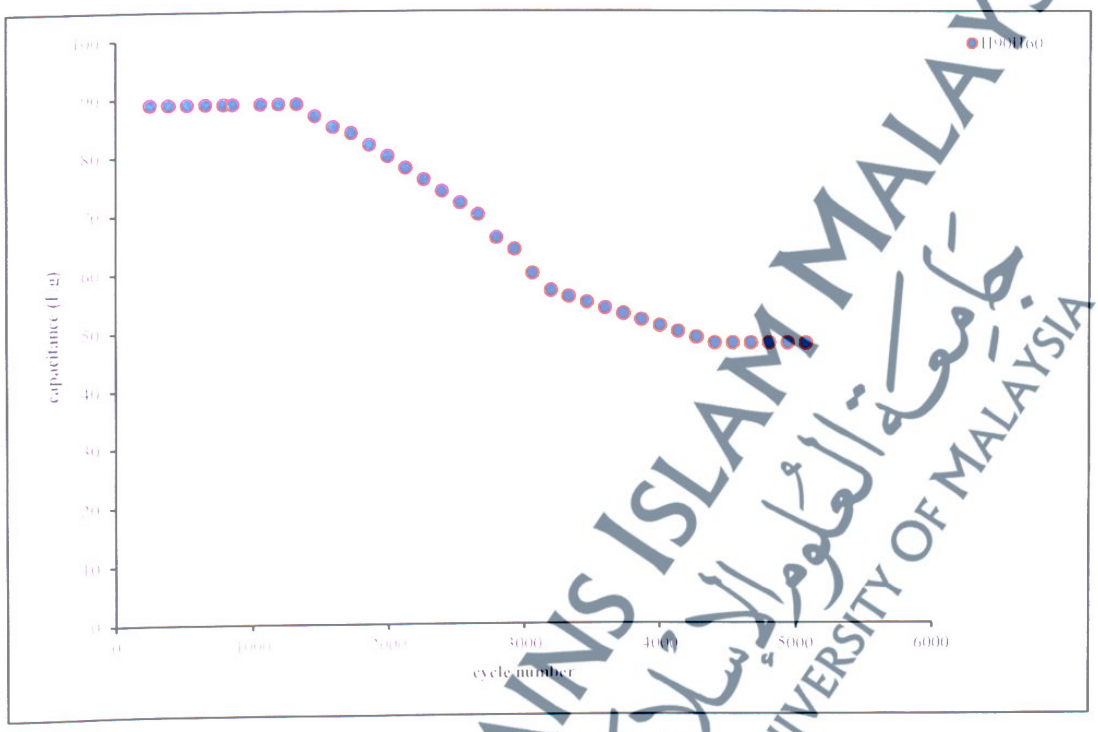

Figure 4.26 Cyclic performances of cell-B (H90PVdF-HFP10 |H60| H90PVdF-HFP10) for a working voltage of 1 V.

Lastly, Fig. 4.27 displayed the cycling endurance measurement over 5000 cycles for the cell C carried out using the CD test at the working voltage of 1.0 V. Unlike cell A and B, cell C displayed about 62 % capacitance retention of its initial value. It was elaborated earlier that although all the three aforementioned cells were made from hydroxyl CNT and shared common characteristics in terms of outer diameter of >50 nm and surface area of 43 m^2g^{-1}, the electrolytes (H50, H60 and H70) incorporated in the sandwiching, having different conductivities are considered the major contributing factors to their differences in conductivities.

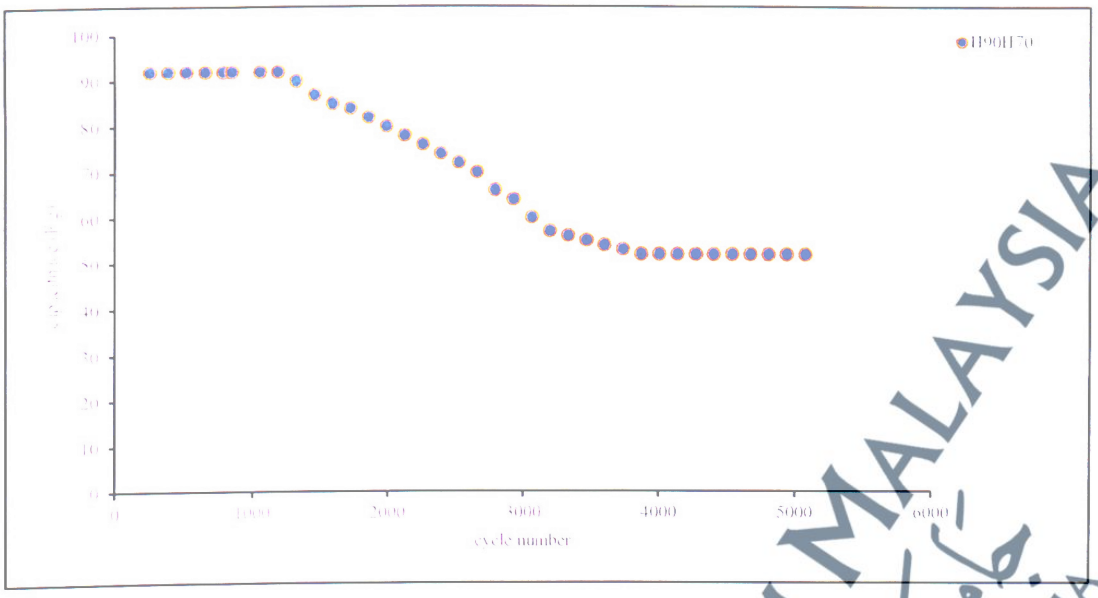

Figure 4.27 Cyclic performances of cell-C (H90PVdF-HFP10 |H70| H90PVdF-HFP10) for a working voltage of 1 V.

The galvanostatic CD test, as earlier mentioned, is considered to be an alternative and arguably better quantitative method to evaluate the supercapacitive nature of an electrode material compared to the CV measurement (Shu et al., 2013).

Following the already mentioned equations, the specific capacitance, energy and power densities, and efficiency of the cells made from CPHMWCNTs and polymer electrolytes (H50, 60 and 70) were calculated using CD analysis.

Fig.4.28 (a) a typical CD profile of cell – A that is made up of an electrode from CPCMWCNTs of the average porous surface area of about 43 m^2g^{-1} and an aqueous hybrid polymer electrolyte of 50 wt. % of the H_3PO_4 of the overall PVA/H_3PO_4 blends (H50) is shown. In order to ascertain the significance of the cell at higher voltage, a voltage range of 0.0 – 1. 0 V was selected. It can be seen that the CD profiles deviate from a typical linear variation of voltage with time that is known for a supercapacitor. This can be associated to the low conductivity of the electrolyte. It can also be observed that the charging and discharging times are almost the same. The specific capacitance

of 9.8, 20.0 and 60.0 Fg^{-1} are obtained at a discharge current of 100, 20 and 10 mA respectively, with a specific energy and power densities of 30.00 Whg^{-1} and 0.11 Wg^{-1} respectively at a discharge current of 100 mA. The overall columbic efficiency of 90.9 % is recorded for this cell. Table 4.14 summarizes all the aforementioned results. There is an IR drop at the beginning of the discharge curve which could be as a result of the porous nature of the electrode and low conductivity of the electrolyte as stated in the earlier discussions.

Based on the CD profile of cell – B depicted in Fig. 4.28 (b) it is evident that, the profile exhibited perfection over that of cell – A. This is attributed to the improvement in the conductivity of the electrolyte. Again, the decrease in ERS can be attributed to the improvement in conductivity because of the carrier induced by the functionalization (Pan et al., 2010). It's charging and discharging times are observed to be same as well, and the specific capacitance of 12.4, 20.0 and 60.0 Fg^{-1} are obtained at a discharge current of 100, 20 and 10 mA respectively, with a specific energy and power densities of 46.5 Whg^{-1} and 0.11 Wg^{-1} respectively, at a discharge current of 100 mA. Its overall columbic efficiency of 90.2 % is recorded (see Table 4.14). However, the IR drop noticed at the beginning of the discharge curve is not as large as that of cell – A which could be as a result of improvement in the conductivity of the electrolyte (i.e. H60).

Fig. 4.28 (c) depicts the CD profile of cell – C, showing a better linear characteristic which imply that there is a formation of good electrode/electrolyte interface with a well-defined conductivity. In addition, the ohmic drop is not as obvious as it in other type of cells. It was also be observed that the charging and discharging times are almost the same. The specific capacitance of 13.2, 47.0 and 99.0 Fg^{-1} are

obtained at a discharge current of 100, 20 and 10 mA respectively, and a specific energy and power densities of 49.50 Whg^{-1} and 0.13 Wg^{-1} respectively, at the said discharge current of 100 mA at the said current applied are also calculated. The overall columbic efficiency of 92.5 % is recorded for this cell (see also Table 4.14).

From the overall results of all the cells, it can be observed from all the cells that, the discharged capacitance decreases with the increase in the applied current, which could be as a result of the low penetration of ions into the inner region of the pores due to fast potential changes.

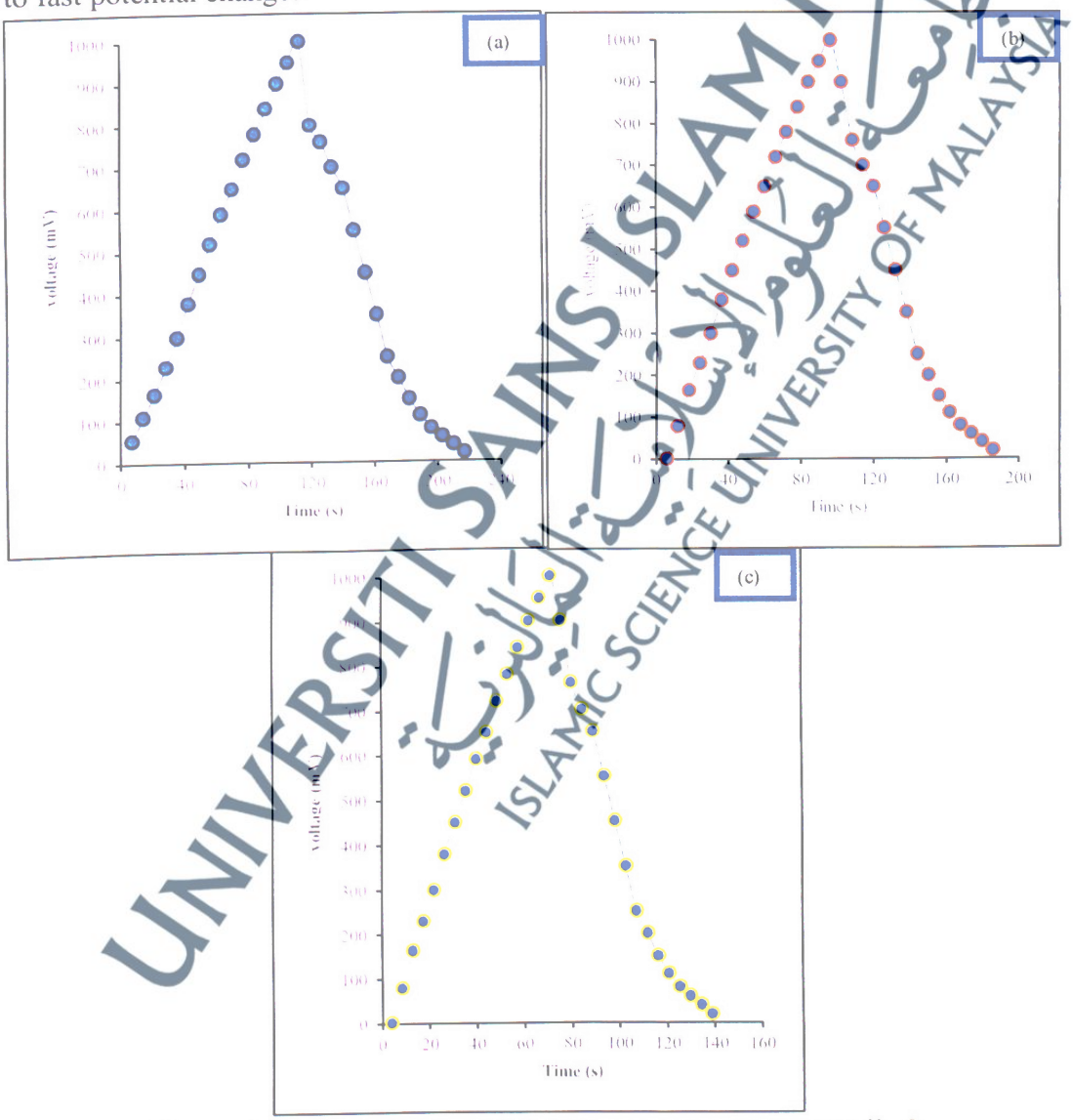

Figure 4.28 CD graphs of **(a)** Cell-A **(b)** Cell-B and **(c)** Cell- C.

Table 4.14 Performances of Supercapacitor by the CD

Cells	Working voltage (V)	C_d (Fg^{-1})	Energy density (Whg^{-1})	Power density (Wg^{-1})	Efficiency (%)
A-H90H50	1	9.8-60.0	30.0	0.11	90.9
B-H90H60	1	12.4-93.0	46.5	0.11	91.2
C-H90H70	1	13.2-99.0	49.5	0.13	92.5

This section demonstrated the fabrication of a CPHWMCNTs used as an electrode for high performance supercapacitors using HPSE which function as an electrolyte and a separator. Three cells were successfully fabricated which were labeled as cell-A (H90PVdF-HFP10 |H50| H90PVdF-HFP10, cell-B (H90PVdF-HFP10 |H60| H90PVdF-HFP10 and cell-C (H90PVdF-HFP10 |H70| H90PVdF-HFP10) with modifications in the separator. The XRD analysis conducted, depicts the peaks of the sample electrode C90PVdF-HFP10 appearing at $2\theta = 26^0$ and 43^0 which might be as a result of the hexagonal structure of (002) and (101) respectively, which is an indication that, the hydroxyl Multiwalled CNT have high conductivity. Again, a wider diffraction at $2\theta = 20.1^0$ which correspond to crystalline peaks of PVDF. TGA traces shows that, the pure CPHMWCNTs experienced a major loss of just 10.1 %, occurring at 696.6 ^{0}C leaving a residue of 88.7 %, which also prove that pure MWCNT have very good thermal stability and consequently, good, in application for electrochemical devices.

From the overall results of the electrochemical analysis of the CV, cell – C delivered highest capacitance of 92 Fg^{-1} by more than 3 folds over cells A and B. This result, as mentioned earlier, is attributed to the remarkable increase in conductivity of the electrolyte used (H70) which has the highest conductivity over H50 and H60 used in the assembly of cell A and B respectively. This was further proved by the CD analysis where cell – C shows a better linear characteristic implying a formation of good

electrode/electrolyte interface with a well-defined conductivity with a very little IR drop observed in the profile, and delivering the highest specific capacitance of 99 Fg^{-1} and a specific energy and power densities of 49.50 Whg^{-1} and 0.13 Wg^{-1} respectively, and attained the overall columbic efficiency of 92.5 %.

In the next section, fabrication of supercapacitor now using an un-functionalized commercial CNTs (CPNMWCNTs) will be explored. Three different types of cells will be assembled with three different kinds of electrolytes (H50, H60 and H70) of different electrical conductivities as separators. Furthermore, all the characterizations and other measurements that were conducted to the foregoing cells fabrications will as well be carried out in this CPNMWCNTs. Notable among them are the CV and CD where effective capacitance, power and energy densities, and efficiency of the cells will all be analyzed.

4.4 Fabrication and Characterizations of Supercapacitor Based on the Commercially Prepared Normal Multiwalled Carbon Nanotubes (CPNMWCNTs) and Hybrid Solid Polymer Electrolytes (HSPE)

4.4.1 Microstructure Characterizations

It was earlier stated that, the XRD spectra were obtained with an XRD (Philip X'Pert XRD with Cu K_α radiation of wavelength λ=1. 54056 Å for 2θ angles between 10° and 80°) that used Cu Kα radiation (λ = 1.5406 Å) operating at 40 kV and 30 mA.

In Fig. 4.29 the XRD analysis of the as-prepared commercial MWCNTs is shown. It can be noticed from this figure that all diffraction peaks can be observed and the major diffraction peaks of the CPNMWCNTs can also be clearly seen. The first two points, peaks that appeared at $2\theta = 26^0$ and $2\theta = 43^0$ which matched with (002) and (101) respectively that the presence of MWCNTs, while the last point on the right side, i.e. $2\theta = 56.1^0$ (also red vertical lines) might be also considered part of the commercial CNT.

The intensity of the peak also indicates that, this as-prepared MWCNTs has high conductivity (Dong et al., 2007) and can be used as carbon electrode. While the first diffracted peak left hand side at $2\theta=20.1^0$ (blue vertical line) correspond to the crystalline peaks of PVdF (Stolarska et al., 2007). Similar XRD results were obtained by (Stolarska et al., 2007; Li et al., 2010). It can be recalled that this powdered CNTs has been identified by suppliers as having high conductivity of 10^2 Scm^{-1}.

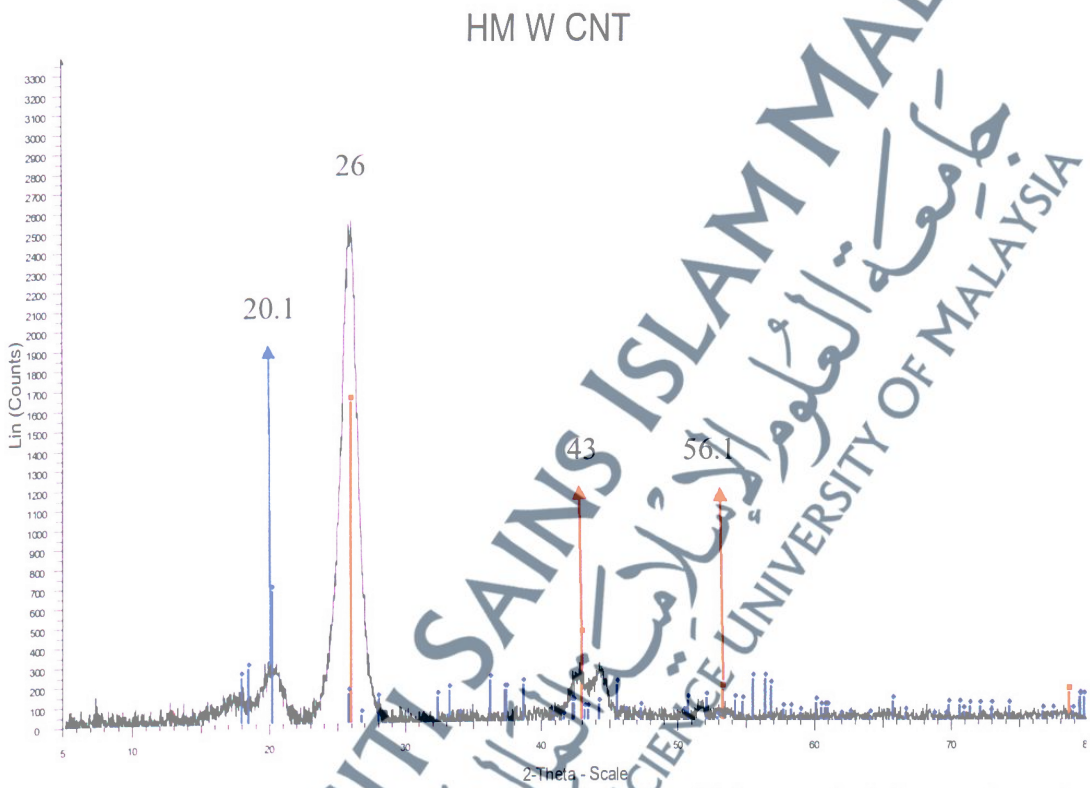

Figure 4.29 XRD plot of CPNMWCNTs with red and blue vertical lines. The red vertical lines indicate the presence of CNTs, while blue lines indicate the presence of PVdF.

For the FESEM analysis, Fig. 4.30 (a) and (b), shows the images of pure CPNMWCNTs (free) and a sample with 90 wt.% of CPNMWCNTs (i.e. N90PVdF-HFP10) respectively. In the case of Fig. 4.30 (a), the image can be said to exhibit similar, regular, entangled and smooth surface morphology with the outer diameter of ~20 nm and lengths of several micrometers. However, when 10 % of a binder was

added to the sample, the agglomeration of the mixture CNTs/binder made the entangling nature of the CNT not to be noticed, which is an indication that, the Normal MWCNTs is more easily mixed with other active materials than the two other functionalized CNTs.

Figure 4.30 FESEM images of **(a)** pure (free) CPNMWCNTs and **(b)** sample with 90 wt.% of CPNMWCNTs (N90PVdF-HFP10) showing an average outer diameter of the tubes. The magnifications of the two samples were 4.3 mm x 150 k and 3.6 mm x 150 k respectively.

Moreover, Fig. 4.31 depicts the FESEM images of N90PVdF-HFP10 electrode overlapped on cellulose HSPE containing 60 wt.% of the H_3PO_4 (H60) at the magnifications of 2.0 kV x 100 k (500 nm). This image was also taken at an angle of 30^0 in order to examine the edge contact at the electrode and electrolyte. As mentioned earlier the reason behind the image taken is to deduce the required needed thickness during the sandwiching of the electrolytes between the electrolytes in order to avoid high resistance and consequent low conductivity of the assembled cell. Hence, in order to overcome above problems, the thickness of the electrode need to be kept at minimum microns, so that ions would be able to diffuse thoroughly from one barrier of the electrode to the other. It was stated in the literature review how different researchers emphasized and recommended that for a high capacitance to be realized, especially in a flexible-type cell, a thinner-liked electrode should be constructed.

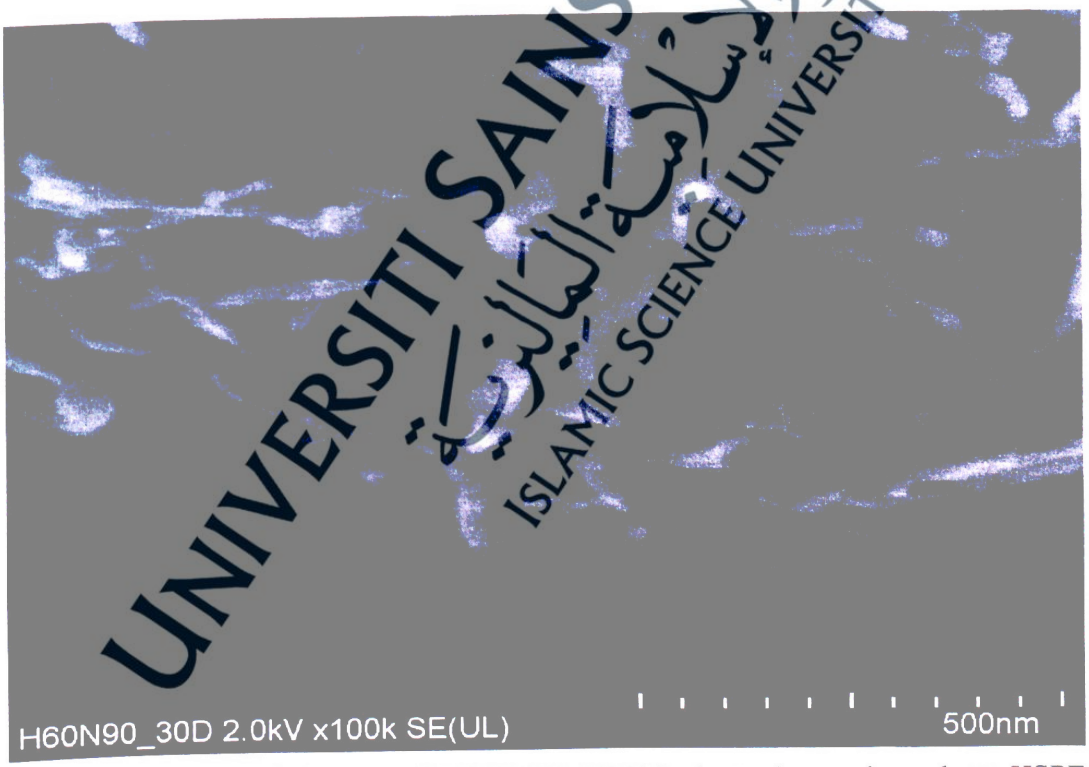

Figure 4.31 FESEM images of N90PVdF-HFP10 electrode overlapped on HSPE containing 60 wt.% of H_3PO_4, 90 wt.% of CPNMWCNTs at the magnifications of 2.0 kV x 100 k (500 nm) and an angle of 30^0.

4.4.2 Thermogravimetric Analysis (TGA)

Using thermal analyzer in the scale-range of 50 ^{0}C to 1000 ^{0}C under nitrogen gas (N_2) flow at a heating rate of 10 ^{0}C min^{-1} on a METTLER, STAR^e SW 10.00, the analysis of the temperature stability of the sample were investigated. This optimum temperature of 1000 ^{0}C was selected knowing that a conventional commercial CNTs should be able to adapt to a temperature greater than 800 ^{0}C. Similar techniques have been shown elsewhere in (Hashim et al., 2014). The thermal stability of the samples was discerned in Fig. 4.31. These figures include (a) 0 wt.% sample (Background) (b) pure NPCWMCNTs (c) N90PVdF-HFP10 – Double scale.

In order to clear any ruminant residue and for re-calibration, the background heating was analyzed. From the traces in Fig. 4.32 (b), it can be seen that, the pure NPCWMCNTs with major loss of just 3.1 % occurring at 596.6 ^{0}C leaving a residue of 94.4 %. However, when the 10 wt.% of the binder was added to the as-prepared sample, the results dramatically change, especially when compared with those of the functionalized CNTs. Fig. 4.32 (b) and (c), provided the thermal stability results. In this case, the two losses were discovered. The initial loss of 4.1 % of the total samples occurs at 108.5 ^{0}C, then the second and major loss was 60.1 % occurred at 745.8 ^{0}C.

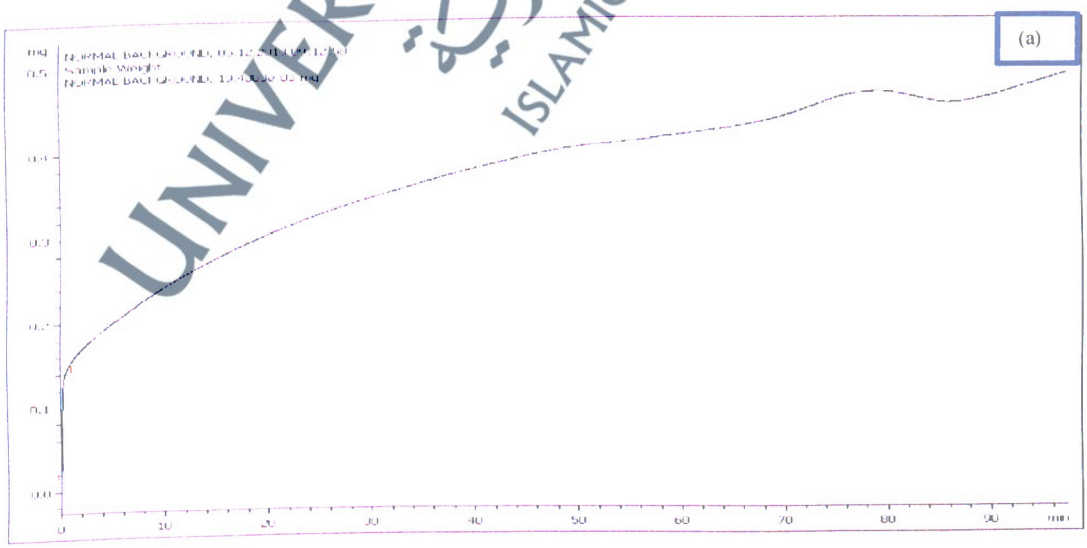

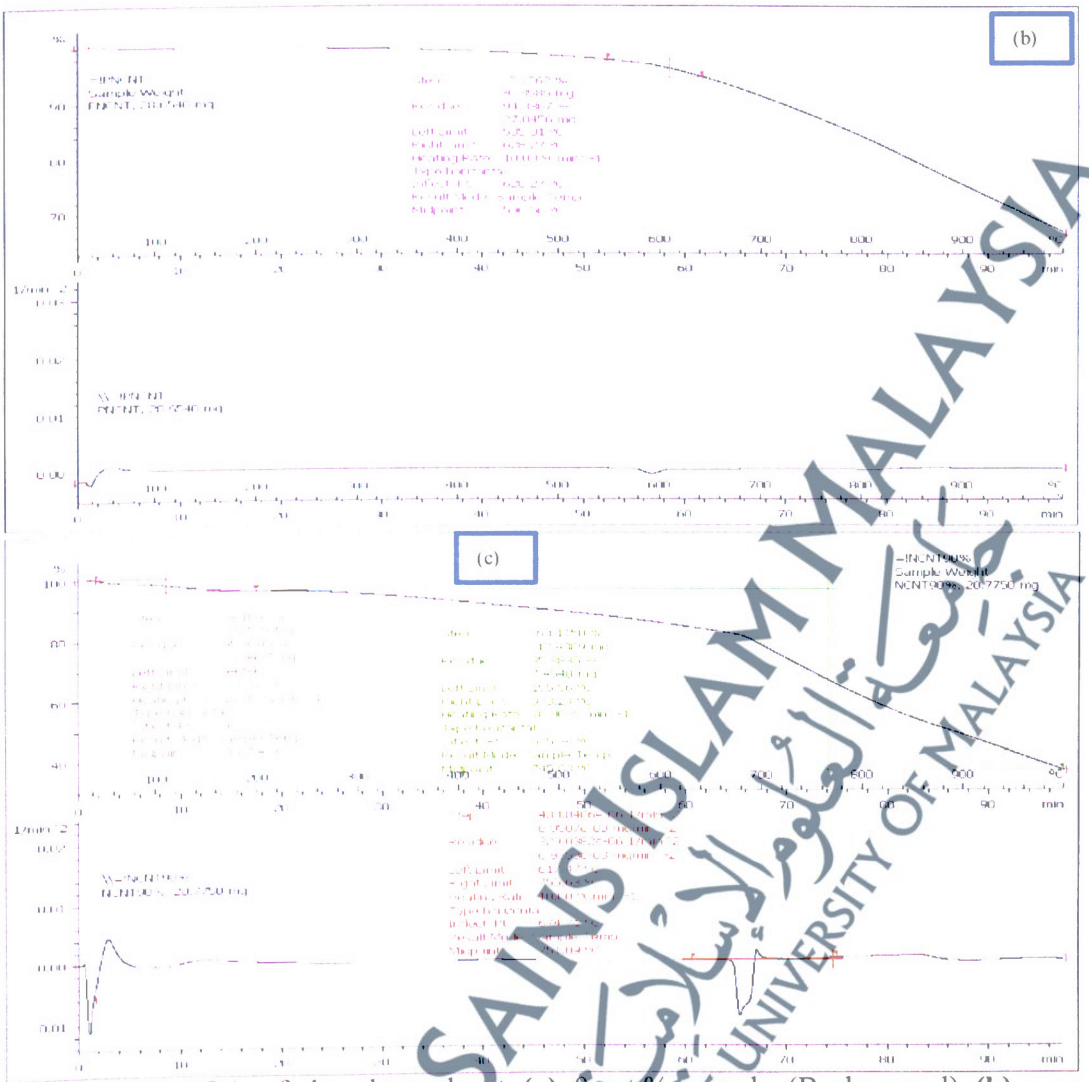

Figure 4.32 TGA of the electrode at **(a)** 0 wt.% sample (Background) **(b)** pure CPNWMCNT **(c)** N90PVdF-HFP10 – Double scale.

4.4.3 Electrochemical Behavior

The electrochemical behaviors of cells constructed by sandwiching the electrode and electrolyte using two-electrode system are therefore investigated by CV and CD measurements. The electrode being a slurry of 90 wt.% of CPNMWCNTs and 10 wt.% of PVdF-HFP. On the other hand, the electrolytes are the three most effective samples, in terms of conductivity among the HSPE that were investigated at the beginning of this chapter. They are the samples with 50, 60 and 70 wt.% of the orthophosphoric acid, which are also coded as H50, H60 and H70 respectively.

Fig. 4.33 shows CV of Cell –A (N90PVdF-HFP10 |H50| N90PVdF-HFP10) at the scan rates of 10, 50 and 100 mV, within a voltage window of 0.0 – 1.0 V. It can be discerned that the resulting CV curves of the cell displayed a leaf-like and mirror symmetric indicating though, a modest supercapacitive behavior for CPNMWCNTs that uses an aqueous electrolyte of 50 wt.% of H_3PO_4 in homogenous solution of PVA/H_3PO_4. The specific capacitance of the electrode materials obtained in the two-electrode system was calculated by integrating the CV curves in the Fig. using the equation that has been stated earlier, in the previous chapter. It could be obtained from the calculations that, the specific capacitance (C_e) of this cell is 30, 50 and 110 Fg^{-1} for the scan rates of 100, 50 and 10 mV respectively as shown in Table 4.15. From these results it can be deduced that, there exist a relationship between the capacitance and scan rate. The specific capacitance decreases from 110 Fg^{-1} to 30 Fg^{-1} which could be attributed to the slow transfer of ions on the electrode electrolyte interface (Shu et al., 2013). Since the electrolytic, film used in this cell fabrication is of low conductivity (H50), this may be evident of the cell performance.

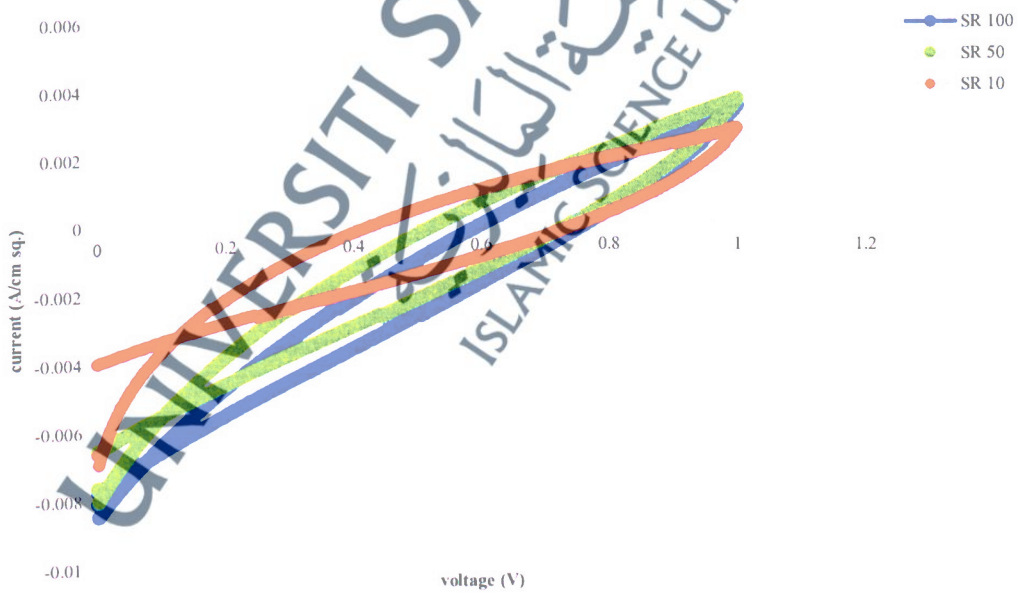

Figure 4.33 CV of Cell –A (N90PVdF-HFP10 |H50| N90PVdF-HFP10) at the scan rates of 10, 50 and 100 mV.

Table 4.15 CV Performances of cell-A (N90PVdF-HFP10 |H50| N90PVdF-HFP10)

Cell	Working voltage (V)	Capacitance value of different scan rates (Fg^{-1})		
		100 mV	50 mV	10 mV
A-N90H50	1	30	50	110

Furthermore, Fig. 4.34 shows CV of Cell–B (N90PVdF-HFP10 |H60| N90PVdF-HFP10) at the scan rates of 10, 50 and 100 mV for a voltage window of 0.0 – 1.0 V. Noting from this cell, the electrolyte used (H60), its specific capacitances improved remarkably to 50, 74 and 158 Fg^{-1} for scan rates of 10, 50 and 100 mV respectively (see Table 4.16). These results almost double that of cell-A which might be attributed to the increase in ionic conductivity in the polymer electrolyte of the HSPE. Unlike the curves of cell A, the resulting CV curves of this cell displayed a better leaf-like and mirror symmetric indicating a modest supercapacitive behavior for a CPNMWCNTs that uses an aqueous electrolyte of 60 wt.% of H_3PO_4 in homogenous solution of PVA/H_3PO_4.

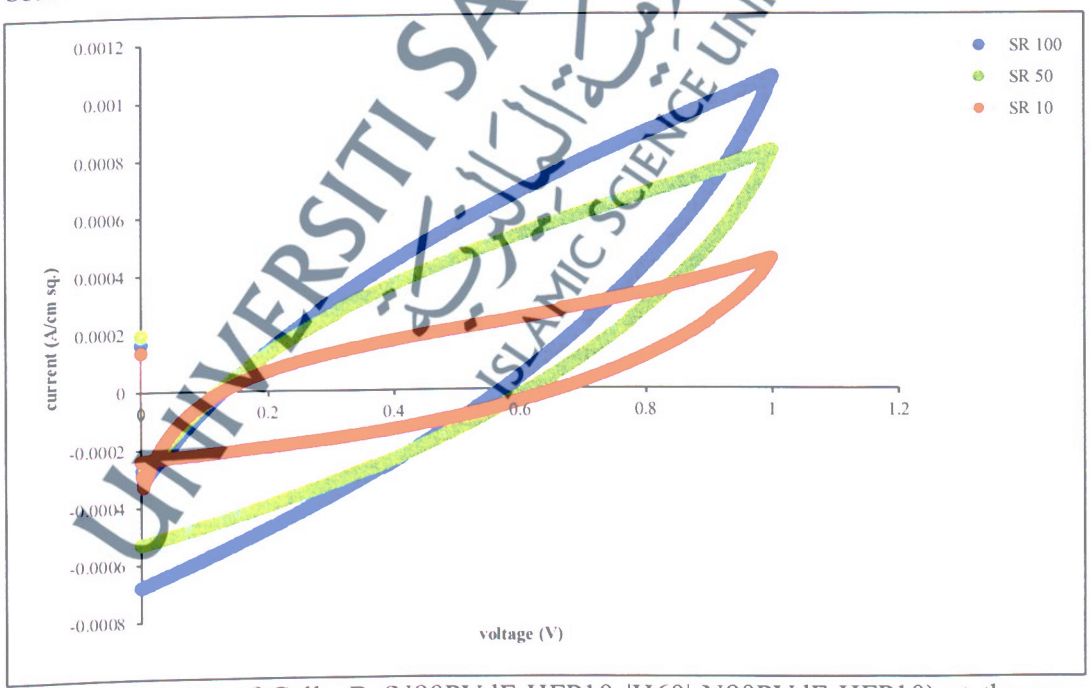

Figure 4.34 CV of Cell –B (N90PVdF-HFP10 |H60| N90PVdF-HFP10) at the scan rates of 10, 50 and 100 mV.

Table 4.16 CV Performances of cell-A (N90PVdF-HFP10 |H60| N90PVdF-HFP10)

Cell	Working voltage (V)	Capacitance value of different scan rates (Fg^{-1})		
		100 mV	50 mV	10 mV
B-N90H60	1	50	74	158

The CV of Cell –C (C90PVdF-HFP10 |H70| C90PVdF-HFP10) at the scan rates of 10, 50 and 100 mV for a voltage window of 0.0 – 1.0 V displayed in Fig. 4.35. This is best performed cell, as it can be noticed from Table 4.17 the capacitance delivery increased remarkably to 59, 91 and 229 Fg^{-1} for the same scan rates of 100, 50 and 10 mV respectively. It can also be discerned that the resulting CV curves of this cell displayed a better leaf-like and mirror symmetric indicating an ideal supercapacitive behavior for CPNMWCNTs in an aqueous electrolyte of 70 wt.% of H_3PO_4 in homogenous solution of PVA/H_3PO_4.

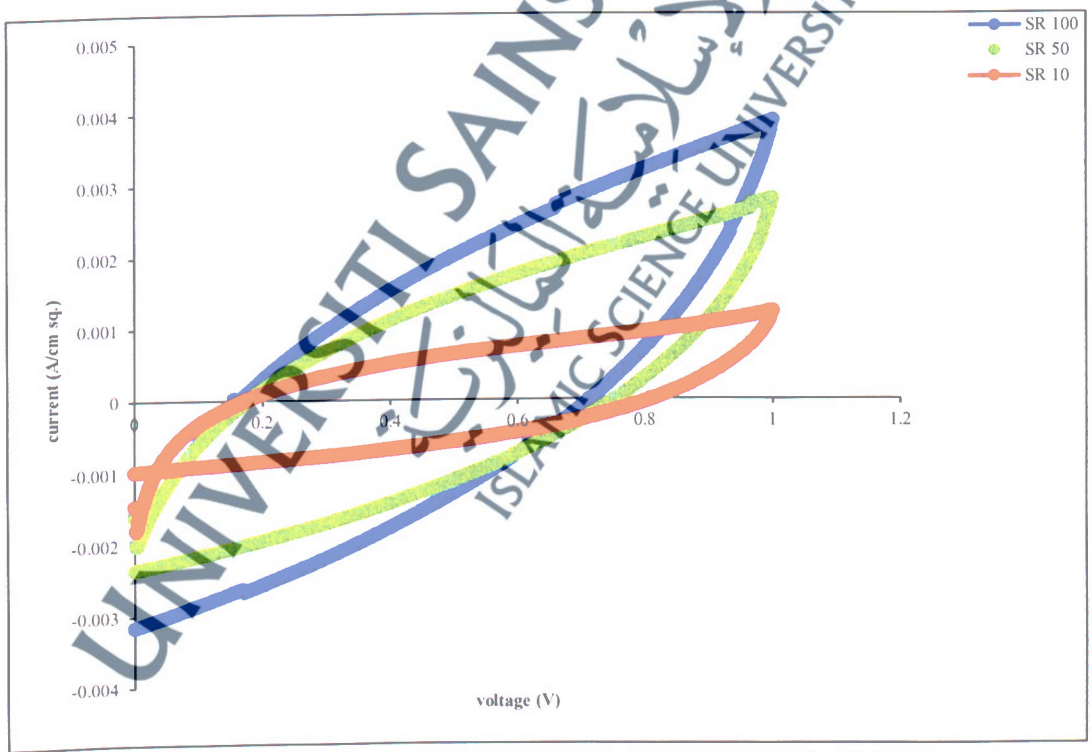

Figure 4.35 CV of Cell –C (N90PVdF-HFP10 |H70| N90PVdF-HFP10) at the scan rates of 10, 50 and 100 mV.

Table 4.17 Performances of Cell –C (N90PVdF-HFP10 |H70| N90PVdF-HFP10)

Cell	Working voltage (V)	Capacitance value of different scan rates (Fg^{-1})		
		100 mV	50 mV	10 mV
C-N90H70	1	59	91	229

As earlier stated, that, it is one of the benchmarks in supercapacitor's fabrication and application to have the ability to endure long term cycling stability. In view of this, Fig. 4.36 shows the cycling endurance measurement over 5000 cycles for the cell – A which was conducted using the CD test at the working voltage of 1.0 V. The Fig. displayed a graph of resulting capacitance as a function of cycling number. It can be seen from the graph that, the cell exhibits the best cycling stability with only about 30 % capacitance retention of its initial value after 5000 cycles. Although the surface area of this electrode is not small (43 m^2g^{-1}), the outer diameter as observed from the FESEM result was about 20 nm. All these, couples with the low conductivity of the polymer electrolytes could possibly be some of the factors that hinder the performance of this cell.

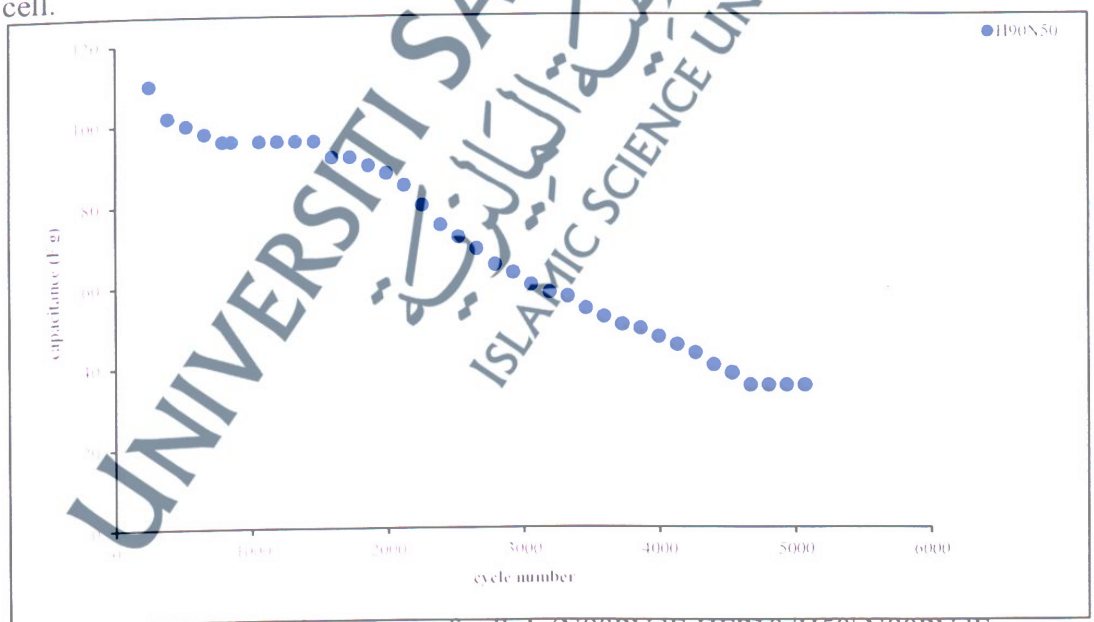

Figure 4.36 Cyclic performances of cell-A (N90PVdF-HFP10 |H50| N90PVdF-HFP10) for a working voltage of 1 V.

While, based on the graph in Fig. 4.37 which displayed the cycling endurance measurement over 5000 cycles for the cell – B, conducted using the CD test at the working voltage of 1.0 V, it can be seen that, compared to cell – A, cell – B which has higher capacitance over cell showcased the best cycling stability, losing about 20 % of capacitance after first 2000 cycles and about 30 % capacitance retention of its initial value after 5000 cycles. Although the conductivity of the separator is higher compared to that of cell – A, this result still shows that the inability of the ions to diffuse through the electrode/electrolyte interface could be part of the factors affecting the stability of the cell.

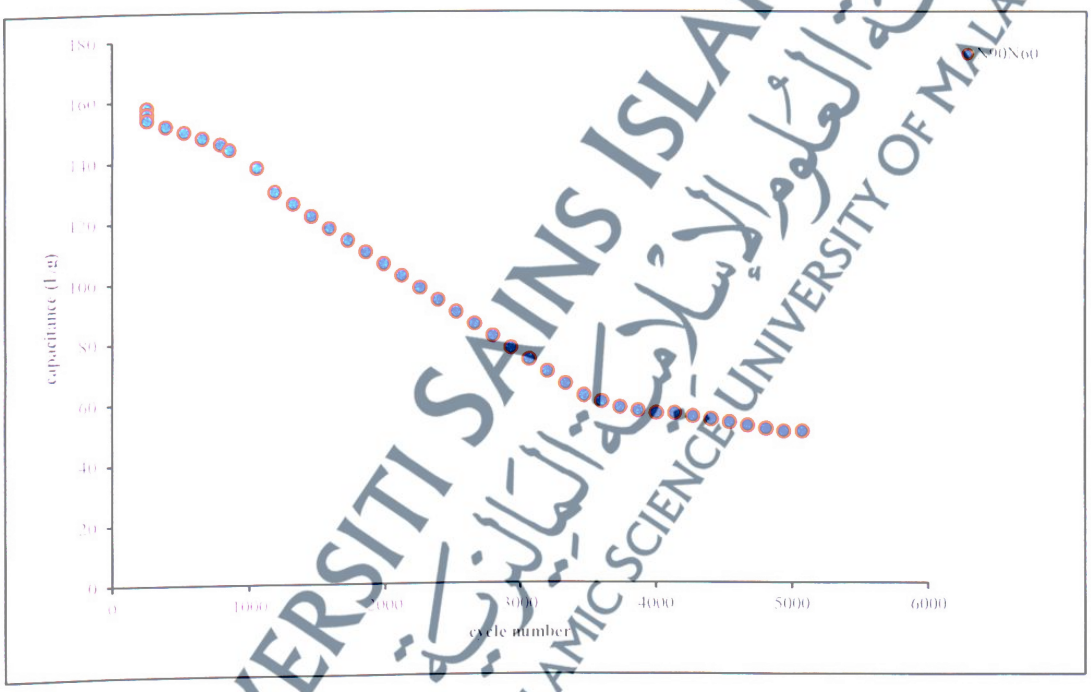

Figure 4.37 Cyclic performances of cell-B (N90PVdF-HFP10 |H60| N90PVdF-HFP10) for a working voltage of 1 V.

Moreover, Fig. 4.38 displayed the cycling endurance measurement over 5000 cycles for the cell – C carried out using the CD test at the working voltage of 1.0 V. This cell started well in the first 1000 cycles, losing less than 5 % of its capacitance. However, after 2000 cycles the cell capacitance retention lowered to about 20 % of its

initial capacitance. Overall, the cell displayed about 38 % capacitance retention of its initial value. As mentioned before, the effect of pore size on this electrode and ionic transfer through the interface of the electrode/electrolyte are the contributing factors of the cell instability. It could be recalled that, the functionalized CNTs displayed, to some extent, better capacitance retention due to their wider pore sizes, thereby increasing the smooth movement of ions at the electrode and electrolyte interface.

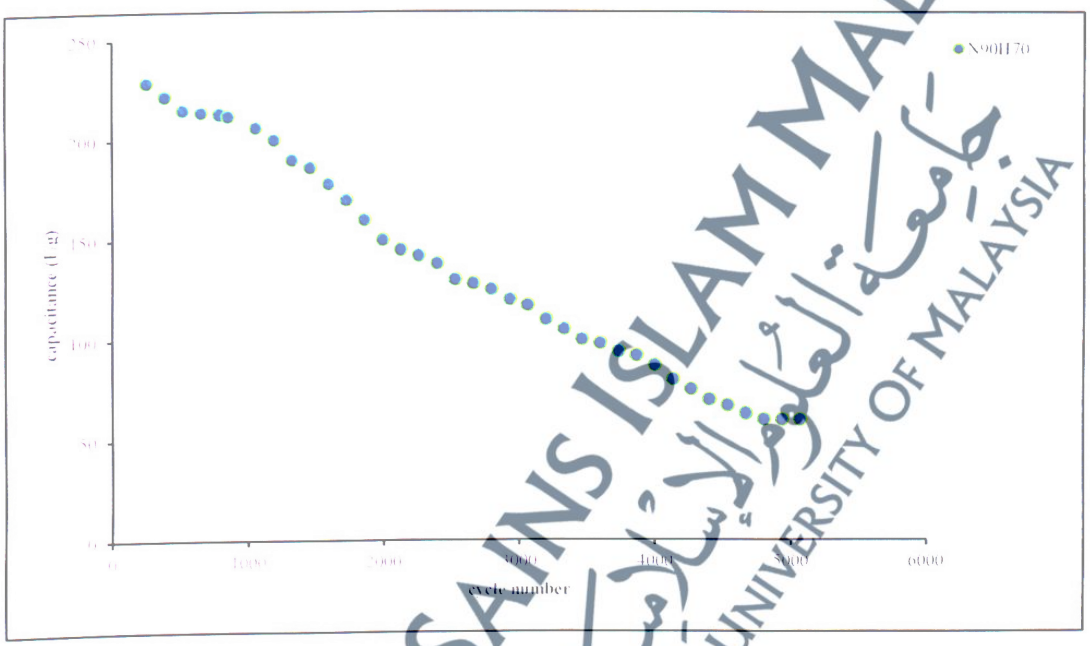

Figure 4.38 Cyclic performances of cell-C (N90PVdF-HFP10 |H70| N90PVdF-HFP10) for a working voltage of 1 V.

Furthermore, to determine the capacitance value and observed the behavior of CD curve, a galvanostatic CD was performed. In Fig. 4.39, the CD graphs of (a) Cell-A (b) Cell-B and (c) Cell- C were all depicted at a working voltage of 1.0 V and at three different discharge current (i.e. 10, 20 and 100 mA). Furthermore, power and energy densities and efficiency of the cells are also calculated.

In Fig.4.39 (a) a typical CD profile of cell – A that is made up of an electrode from CPCMWCNTs of the average porous surface area of about 43 m^2g^{-1} and an aqueous hybrid polymer electrolyte of 50 wt.% of the H_3PO_4 of the overall PVA/H_3PO_4

blends (H50) is shown. A voltage range of 0.0 – 1. 0 V was selected in order to determine the significance of the cell at higher voltage. It can be seen that the CD profiles deviate from a typical linear variation of voltage with time that is known for a supercapacitor. The observed non-linearity can be attributed to the low conductivity of the electrolyte. It can also be observed that the charging and discharging times are closely the same. The specific capacitance of 13.4, 33.5 and 100.5 Fg^{-1} are obtained at a discharge current of 100, 20 and 10 mA respectively, with a specific energy and power densities of 50.25 Whg^{-1} and 0.08 Wg^{-1} respectively, at a discharge current of 100 mA. The overall columbic efficiency of 86.5 % is recorded for this cell (see Table 4.18). The large IR drop at the beginning of the discharge curve could be as a result of the porous nature of the electrode or low conductivity of the electrolyte or both.

Furthermore, Fig. 4.39 (b) shows a CD profile of cell – B. Although, the variation of voltage with respect to time is again not linear, however, the profile looks better than that of cell – A. This could be as a result of improvement in the conductivity of the electrolyte. The specific capacitance of 16.6, 14.5 and 124.5 Fg^{-1} are obtained, at a discharge current of 100, 20 and 10 mA respectively, and a specific energy and power densities of 62.5 Whg^{-1} and 0.13 Wg^{-1} respectively, at a discharge current of 100 mA. Its overall columbic efficiency of 87.8 % is recorded (as shown in Table 4.18). However, the voltage drop noticed at the beginning of the discharge curve is as significant as in the case of cell – A which could be attributed to the significant improvement in the conductivity of the electrolyte.

Last but not the least is the CD profile of cell – C depicted Fig 4.39 (c) showing perfect linear characteristic implying a formation of good electrode/electrolyte interface with a good conductivity. Again, no ohmic drop is observed in this case. Three different

applied currents for the measurement have been employed. It was also be observed that the charging and discharging times are almost the same and better than those of cell – A and C. The specific capacitance of 18.8, 47.0 and 141.0 Fg^{-1} are obtained at the discharge currents of 100, 20 and 10 mA respectively. While the specific energy and power densities of 70.50 Whg^{-1} and 1.00 Wg^{-1} respectively, at the said discharge current of 100 mA are also calculated. The overall columbic efficiency of this cell is 90.2 %.

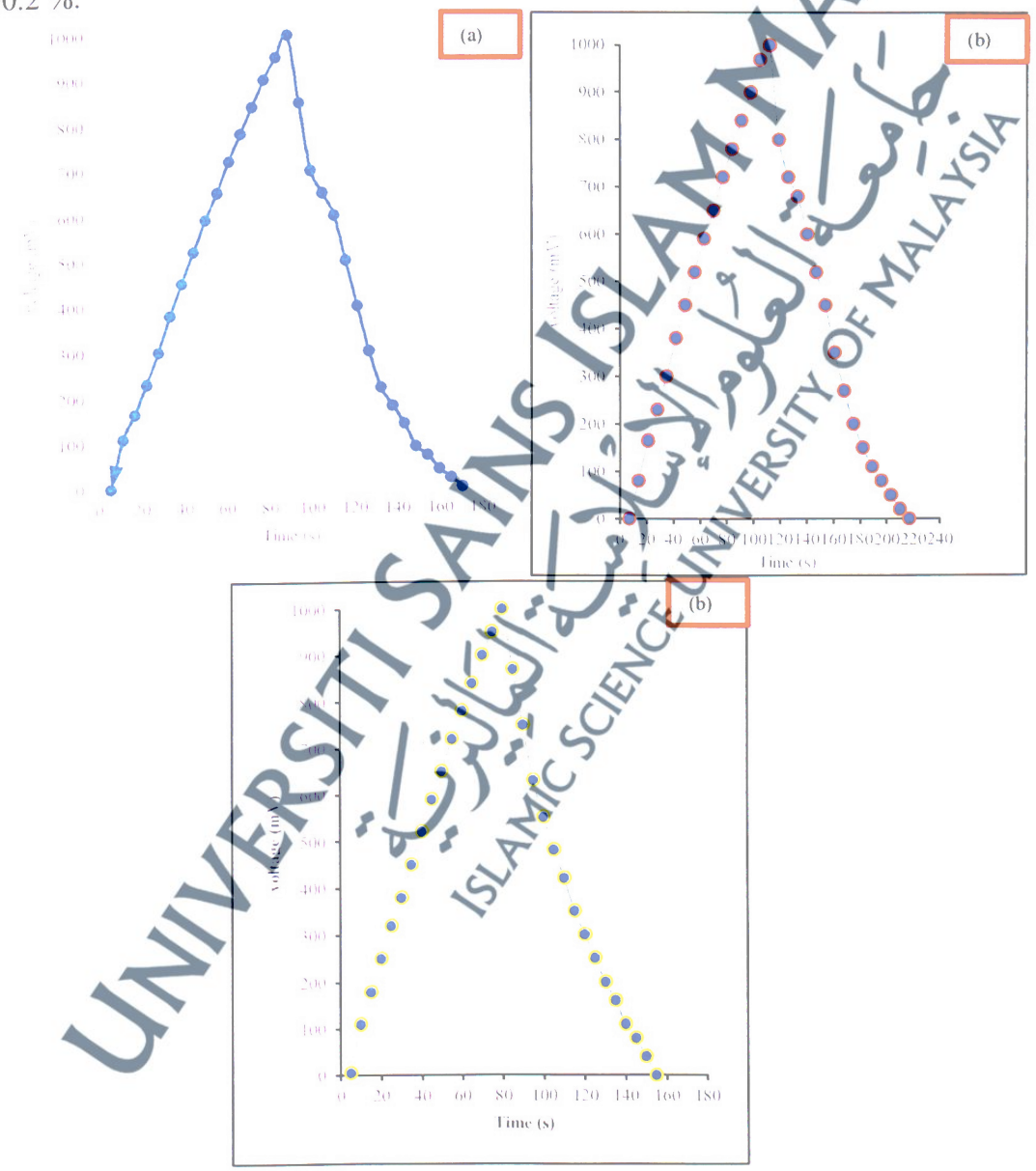

Figure 4.39 CD graphs of **(a)** Cell-A **(b)** Cell-B and **(c)** Cell- C

Table 4.18 Performances of Supercapacitor by the CD

Cells	Working voltage (V)	C_d (Fg^{-1})	Energy density (Whg^{-1})	Power density (Wg^{-1})	Efficiency (%)
A-N90H50	1	13.4-101	50.25	0.08	86.5
B-N90H60	1	16.6-125	62.25	0.13	87.8
C-N90H70	1	18.8-141	70.50	1.00	90.2

To conclude this section, a fabrication of CPNMWCNTs/PVDF-HFP used as an electrode for high performance supercapacitors using HPSE of three different conductivities (H50, H60 and H70) was discussed. All the three cells were successfully fabricated and were labeled as cell-A (H90PVdF-HFP10 |H50| N90PVdF-HFP10), cell-B (N90PVdF-HFP10 |H60| N90PVdF-HFP10) and cell-C (N90PVdF-HFP10 |H70| N90PVdF-HFP10). Several analyses such as FESEM, XRD, TGA and electrochemical analysis were carried out. From the overall of the electrochemical analysis of CV results, cell-C delivered the highest capacitance of 229 Fg^{-1}. While for the CD analysis of all the cells conducted within a voltage window of 1.0 V, cell-C also delivered better discharge capacitance of 144 Fg^{-1} with highest energy and power densities of 70.50 Whg^{-1} and 1.00 Wg^{-1} respectively. The cell efficiency was calculated to be 90.2 %.